Mon. Not. R. Astron. Soc. **272,** 800–820 (1995)

The formation of bipolar planetary nebulae and close white dwarf binaries

Zhanwen Han, Philipp Podsiadlowski and Peter P. Eggleton
Institute of Astronomy, Madingley Road, Cambridge CB3 0HA

Accepted 1994 September 17. Received 1994 July 18

ABSTRACT

We systematically investigate the effects of binary interactions on the formation and shaping of planetary nebulae (PNe) and the various evolutionary channels leading to the formation of close white dwarf binaries, in particular cataclysmic variables (CVs), double degenerate binaries (DDs) and potential progenitors of Type Ia supernovae (SNe). Using Monte Carlo simulations, we explore the consequences of various binary mass-ratio distributions, different initial–final mass relations, different population parameters (such as age and metallicity), and different theoretical assumptions concerning the modelling of the common-envelope phase.

Our results agree well with observations and – where comparable – with previous studies. Our main conclusions are the following. (1) The morphology of 34 to 43 per cent of all planetary nebulae is affected by binary interactions, if we assume that 50 per cent of all stellar systems are binaries with orbital periods less than ~100 yr. (2) The main types of binary interactions considered (gravitational focusing, common-envelope ejection and binary merger) are all of comparable importance. (3) Massive binaries are slightly more likely to produce bipolar PNe, provided that the initial mass-ratio distribution is biased towards a mass ratio near unity. (4) The orbital periods of close white dwarf binaries that experienced a common-envelope (CE) phase extend to longer orbital periods than found in earlier studies, because the binding energy of the CE of initially wide systems is reduced. (5) Best agreement with observations, in particular the fraction of PNe with close binary nuclei and the birth rates of CVs and DDs, is obtained if the process that leads to the ejection of CEs is very efficient. (6) The rate of mergers of two CO white dwarfs with a total mass larger than the Chandrasekhar mass, possibly leading to a Type Ia supernova, is marginally consistent with the observational SN Ia rate, although not in our best model. (7) Our simulations support the initial–final mass relation proposed by Han, Podsiadlowski & Eggleton and the use of PNe as a standard distance candle.

Key words: binaries: general – novae, cataclysmic variables – supernovae: general – white dwarfs – planetary nebulae: general.

1 INTRODUCTION

Planetary nebulae (PNe) are shells of low-density ionized gas that have been ejected by their central stars. They play an important role in our understanding of the final stages of stellar evolution and may even be a valuable tool for calibrating the extragalactic distance scale. While most PNe exhibit complex but highly axisymmetric shapes, only a small fraction (~20 per cent) show spherical symmetry; the majority of PNe are either elliptical (~30 per cent) or bipolar (~50 per cent), including ~20 per cent of PNe with butterfly morphology (see, for example, Zuckerman & Gatley 1988). A variety of scenarios has been proposed to explain the shaping of PNe: the most important of these are *the interacting-winds model* (Kwok, Purton & Fitzgerald 1978; Okorokov et al. 1985; Volk & Kwok 1985; see also Pikel'ner 1968, 1973; Kahn & West 1985), *binary interaction models* (Fabian & Hansen 1979; Livio, Salzman & Shaviv 1979; Morris 1981; Kolesnik & Pilyugin 1986; Morris 1987; Pilyugin 1987; Bond & Livio 1990) and *magnetic models* (Pascoli 1987a,b; Chevalier & Luo 1994). For a detailed review and further references, see Podsiadlowski & Clegg

(1992). The interacting-winds model can account for the bipolarity of many PNe if there is a large density contrast in the slow wind (emitted during the asymptotic giant phase) between the equatorial plane and the polar directions. However, this model does not specify the origin of the density contrast. Binary interactions provide a plausible mechanism for producing bipolarity, but it is not clear whether there are enough interacting binaries to account for the large fraction of non-spherical PNe. Magnetic models can also explain bipolar PNe, but seem to require very strong stellar dynamos.

In this paper, we investigate systematically how binary interactions can produce bipolar PNe. Previously, Zuckerman & Aller (1986) concluded that binary interactions could not be a primary cause for the observed non-sphericity of most PNe, since (1) there are not enough binaries and (2) the strongly bipolar PNe tend to be found at lower Galactic latitudes than the average PN, suggesting that they have more massive progenitors. Neither of these arguments can, however, be considered very conclusive. The second argument – the evidence for the spatial separation is actually not very strong – may only imply that bipolar PNe are more likely to be found in *massive binaries* (see Section 6.2). The first argument is also not without its counter-arguments. The most extreme view is represented by Paczyński (1985), who has argued that duplicity may be a prerequisite for the PN phenomenon and that *all* PNe are the product of binary interactions. This hypothesis is almost certainly too extreme, but we note that some sort of binary interaction may be required to account for only the very non-spherical PNe, while most of the elliptical PNe could be the product of single-star evolution.

Here, we will try to take an unbiased, a priori approach: we first determine the various binary evolutionary channels that may be able to influence the morphology of PNe and then examine their importance individually. We use a Monte Carlo method to estimate the a priori probabilities of each channel and to explore the dependence of these estimates on the metallicity and age of the population, the binary parameters, etc. We also keep track of some of the types of binaries formed in the simulations, in particular cataclysmic variables (CVs), double degenerates (DDs) and potential Type Ia supernova progenitors (SNe Ia). This allows us to compare our results with a number of recent independent, but related, studies (e.g. de Kool 1992; Tutukov, Yungelson & Iben 1992; Yungelson et al. 1994). In a subsequent paper, we will discuss in detail the implications and predictions of our simulations for a large variety of binary types (for example barium stars, symbiotic binaries, helium stars, RCrB stars, O/B subdwarfs, etc.).

The outline of this paper is as follows. In Section 2, we describe the adopted stellar models and in Section 3 the evolutionary channels for the formation of PNe, CVs, DDs and SNe Ia. In Section 4, we list the theoretical assumptions of our Monte Carlo simulations and in Section 5 we present the results of the simulations. Finally, in Section 6, we discuss and summarize the implications of these results.

2 STELLAR MODELS

In order to follow the evolution of individual sample stars in a Monte Carlo simulation, we need sets of stellar evolution models from which the required stellar properties can be extracted. In this section, we briefly describe the stellar evolution models, the method for calculating the envelope energy, and the determination of the initial–final mass relation.

2.1 Stellar model grid

We used the latest opacity tables of Rogers & Iglesias (1992), supplemented with molecular opacities at low temperatures from the compilation of Weiss, Keady & Magee (1990), to construct a grid of stellar evolution models for two compositions, a typical Population I (Pop I) composition with hydrogen abundance $X=0.70$, helium abundance $Y=0.28$ and metallicity $Z=0.02$ and a representative Population II (Pop II) composition with $X=0.75$, $Y=0.25$ and $Z=0.001$. For a detailed description of the evolutionary computational method, see Han, Podsiadlowski & Eggleton (1994b, hereafter HPE). The models do not include mass loss and use a ratio of mixing length to pressure scaleheight $\alpha=2$, which gives a reasonable calibration of the models. The model grid for Pop I covers the range from 0.8 $M_\odot$ to 16.0 $M_\odot$ at roughly equal intervals in $\log M$ ($M=0.8$, 1.0, 1.25, 1.60, 2.0, 2.5, 3.0, 4.0, 5.0, 6.3, 8.0, 10.0, 12.5 and 16.0 $M_\odot$). The Pop II model grid is the same, but only goes up to 8 $M_\odot$. The stellar parameters required in the Monte Carlo simulations are calculated at more than 50 points for each evolutionary track in the Hertzsprung–Russell (HR) diagram. To determine the required stellar parameters between grid points, we have devised an interpolation scheme which yields, with reasonable precision, the stellar age, radius, effective temperature, surface luminosity, core mass, core radius, envelope gravitational binding energy and envelope thermal energy.

Fig. 1 shows the HR diagrams for the evolutionary sequences in our model grid for Pop I (a) and Pop II (b); the termination points are indicated according to the different initial–final mass relations in Section 2.3. When the mass of a stellar core reaches the final mass given by the adopted initial–final mass relation, it is assumed that the envelope is ejected, leaving the degenerate core as the central star of a PN and 'terminating' the evolution. For some initial masses, the core masses of our asymptotic giant branch (AGB) models are always larger than the final mass given by the first two initial–final mass relations in Section 2.3; in these cases, we end the evolution when the core mass is closest to the required final mass.

2.2 Envelope energy

The envelope binding energy $E_{\rm env}$ is required in the criterion for common-envelope ejection (see Section 3.3). We take it as

$$E_{\rm env}=E_{\rm gr}-\alpha_{\rm th}E_{\rm th}. \qquad (1)$$

The envelope energy consists of two parts, the thermal energy $E_{\rm th}=\int_{M_c}^{M_s}U\,{\rm d}m$ and the gravitational binding energy $E_{\rm gr}=\int_{M_c}^{M_s}(Gm)/r\,{\rm d}m$, where M_s is the stellar surface mass and M_c the core mass. For practical determination of M_c, see section 2 of HPE. U is the internal energy of thermodynamics, involving terms due to the ionization of H and He and the dissociation of H_2, as well as the basic $3\mathscr{R}T/2\mu$ for a

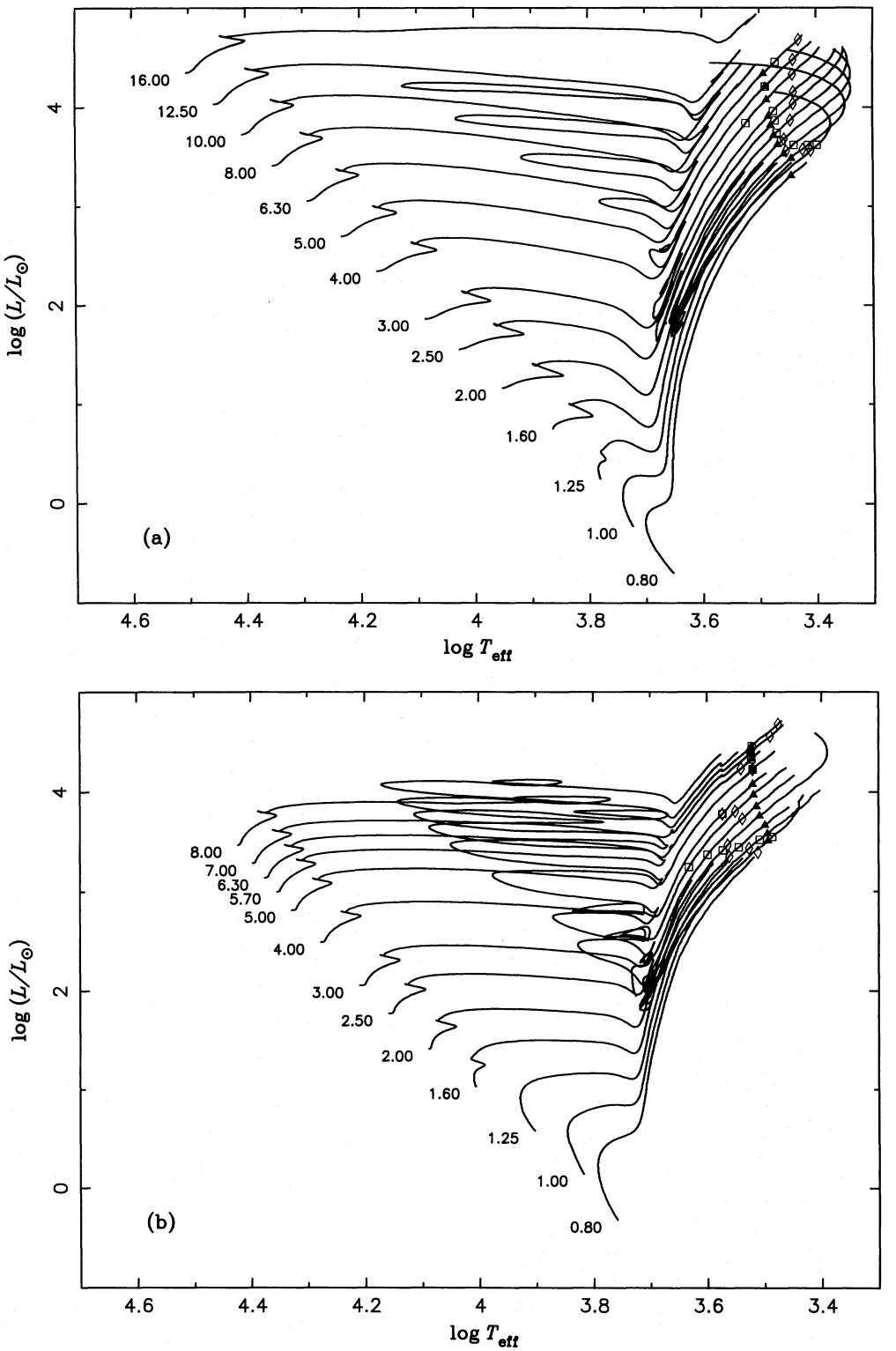

Figure 1. Hertzsprung–Russell (HR) diagrams for the evolutionary sequences in our model grid [(a): Pop I; (b): Pop II]. The end points of the various initial–final mass relations are indicated (dark triangle: HPE relation; square: YTL relation; and diamond: IT relation).

simple perfect gas, the energy of radiation, and the Fermi energy of a degenerate electron gas. In equation (1), we have introduced the parameter $\alpha_{\rm th}$, since it is uncertain what fraction of the thermal energy is used in driving the CE ejection: this depends on the very uncertain details of the ejection process. We generally take $\alpha_{\rm th}$ to be 0.0, 0.5 or 1.0.

2.3 Initial–final mass relations

The evolution of single stars, including those that are formed as a result of the merger of the components of a binary, is terminated according to an initial–final mass relation. We consider the following three initial–final mass relations.

(i) The observational initial–final mass relation of Weidemann & Koester (1983) and Weidemann (1984) in the approximation given by Yungelson, Tutukov & Livio (1993):

$$\log(M_f/M_\odot) = \begin{cases} -0.22 + 0.36[\log(M_i/M_\odot)]^{2.5}, \\ \qquad\qquad \text{if } \log(M_i/M_\odot) > 0; \\ -0.22 - 0.36\,|[\log(M_i/M_\odot)]|^{2.5}, \\ \qquad\qquad \text{if } \log(M_i/M_\odot) \le 0. \end{cases} \quad (2)$$

Subsequently, we refer to this relation as the YTL relation. Note that the semi-empirical relation obtained by Weidemann & Koester is given graphically and contains a considerable spread, so that the YTL relation is only one of several possible formulae that might fit the data equally well.

(ii) The initial–final mass relation proposed by Iben & Tutukov (1984a, hereafter IT), which is close to one obtained by assuming a Reimers' mass loss rate (Reimers 1975) with Reimers' efficiency parameter $\eta = 2$; this is also reasonably close to the one found by Weidemann & Koester (1983) and Weidemann (1984):

$$M_f/M_\odot = 0.446 + 0.106\,M_i/M_\odot. \quad (3)$$

(iii) A theoretical initial–final mass relation proposed by HPE, which is based on the assumption that the envelope is ejected when its binding energy ($E_{gr} - E_{th}$, Section 1.2) changes from positive to negative:

$$\begin{aligned} M_f/M_\odot &= \max[0.54 + 0.042\,M_i/M_\odot, \\ &\quad \min(0.36 + 0.104\,M_i/M_\odot, 0.58 + 0.061\,M_i/M_\odot)], \\ &\quad 1\,M_\odot \le M_i \le 8\,M_\odot, \\ M_f/M_\odot &\simeq 0.46, \quad 0.8\,M_\odot \le M_i \le 1\,M_\odot, \end{aligned} \quad (4)$$

for Pop I ($X = 0.7$, $Y = 0.28$, $Z = 0.02$), and

$$\begin{aligned} M_f/M_\odot &= \max[0.54 + 0.073\,M_i/M_\odot, \\ &\quad \min(0.29 + 0.178\,M_i/M_\odot, 0.65 + 0.062\,M_i/M_\odot)], \\ &\quad 0.8\,M_\odot \le M_i \le 7\,M_\odot, \end{aligned} \quad (5)$$

for Pop II ($X = 0.75$, $Y = 0.25$, $Z = 0.001$).

Even though equations (2) and (3) are only applicable to Pop I, we also use them in some Pop II simulations in order to examine whether there are significant differences between these relations and the HPE relation, which predicts a higher white dwarf mass for a given initial mass for Pop II.

3 EVOLUTIONARY CHANNELS

A successful model for explaining the variety of PN structures is the 'interacting-winds' model (Kwok et al. 1978; Okorokov et al. 1985; Volk et al. 1985). In this model, a red giant first loses most of its envelope in the form of a slow superwind. When the central hot core is exposed, it emits a fast wind which pushes into the slow wind and sweeps it up into a PN shell. Detailed hydrodynamical simulations (e.g. Icke, Preston & Balick 1989; Frank et al. 1993) show that an 'interacting-winds' model can explain the whole range of structures provided that there exists a density contrast in the slow wind between the equatorial plane and the polar directions that varies continuously from one system to another. Typically, an elliptical PN requires a density contrast ~ 2, and a butterfly PN a density contrast larger than ~ 5–10. While this model has been very successful in explaining the observed shapes of PNe, it does not and cannot explain the origin of the large density contrast which is responsible for elliptical and butterfly PNe. In particular, the large density contrast required to produce butterfly PNe suggests that mass loss from some AGB stars resembles more an equatorial (disc-like?) outflow than an oblate wind.

Three main conclusions have been proposed for producing the required density contrasts in AGB winds: stellar rotation, magnetic fields and binary interaction (see the references in Section 1). However, simple angular momentum and magnetic field considerations show that a single star, even if it were rapidly rotating and/or had a strong magnetic field on the main sequence, cannot produce more than a modest density contrast in its wind on the AGB (see Podsiadlowski & Clegg 1992; Livio 1994) and is therefore unlikely to produce a strongly bipolar PN. In the present study, we only consider evolutionary channels that involve binary interactions. In particular, we consider as the main binary channels: detached but close binaries systems, semi-detached binaries, and common-envelope systems.

3.1 Detached binary systems

In a detached binary system, the presence of a companion star will affect the wind emanating from the evolved primary because it provides an attractive force to focus the wind gravitationally even if the wind is spherically symmetric in the primary's reference frame (Fabian & Hansen 1979; Morris 1981; Kolesnik & Pilyugin 1986; Pilyugin 1987). As a consequence, the wind may be focused towards the equatorial plane to produce a disc-like outflow which is then responsible for the PN bipolarity. To estimate the importance of gravitational focusing, Morris (1990) has defined a gravitational focusing fraction (i.e. the fraction of the total mass of the outflow that is focused by the companion) as

$$\alpha_{\rm focus} = \frac{\dot{M}_{\rm focus}}{\dot{M}_{\rm outflow}} = \frac{0.8}{V_w}\left[\frac{M_2}{a}\right]^2\left[V_w^2 + 0.9\,\frac{M_1 + M_2}{a}\right]^{-3/2}, \quad (6)$$

where the primary and secondary masses, M_1 and M_2, are in solar units, the binary separation a is in units of 10 au and the wind velocity V_w is in units of 10 km s^{-1}.

In our calculations, we use a typical wind velocity $V_w = 10$ km s^{-1} (Kwok 1982; Soker & Livio 1989) and define three levels of gravitational focusing: *weak focusing* for $\alpha_{\rm focus} < 0.1$, *mild focusing* for $0.1 < \alpha_{\rm focus} < 0.5$ and *strong focusing* for $\alpha_{\rm focus} > 0.5$. We consider the gravitational focusing effect both when the primary and, later, the secondary (if massive enough) lose their envelopes, and we rather arbitrarily assume that a bipolar PN is produced from mild focusing or strong focusing, but not from weak focusing.

3.2 Semidetached binary systems

A large fraction of binary systems experiences Roche lobe overflow (RLOF) once or several times during their lifetimes. If mass transfer is dynamically stable (Morton 1960), a semi-detached system is formed in which mass is transferred from one star to the other. Observations suggest (e.g. Garcia & Gimenez 1992) that a significant fraction of mass lost by the

mass-losing component is lost from the system, preferentially in the orbital plane. This will then form a disc-like structure around the system and influence the PN structure (Morris 1987). We therefore assume that a bipolar PN is formed whenever the star that is ejecting its envelope is filling its Roche lobe. We also note that *any* Roche-lobe-filling star is a rapid rotator if it is tidally locked to the orbit (see Podsiadlowski & Clegg 1992), and mass loss from it is expected to be rotationally flattened (e.g. Poe & Friend 1986).

While PNe ejected from semidetached systems are likely to be very bipolar, such systems will be relatively rare since mass transfer from an AGB star is generally dynamically unstable (Paczyński & Sienkiewicz 1972) and may lead to a common-envelope phase (Section 3.3). On the other hand, there is ample observational evidence (e.g. Webbink 1986; Morris 1987; Eggleton & Tout 1989; Podsiadlowski, Joss & Hsu 1992) that there are several classes of binaries in which mass transfer takes place from a star with a deep convective envelope without leading to a common-envelope phase. A likely explanation for this is that, in these systems, the mass donor has already lost a significant amount of mass before the onset of RLOF in a stellar wind (possibly enhanced in flux owing to the presence of a close binary companion; Tout & Eggleton 1988). Dynamical mass transfer can then be avoided, provided that the initial mass ratio was close to unity. In our simulations, stellar winds are not included. Therefore this channel for the formation of bipolar PNe is completely insignificant and will not be discussed any further. If stellar winds and, in particular, binary-enhanced stellar winds are taken into account, one might expect up to a few per cent of bipolar PNe to originate in semidetached systems.

3.3 Common-envelope binary systems

When the Roche-lobe-filling star has a deep convective envelope (for example during its giant phase), mass transfer is generally dynamically unstable if the mass ratio M_1/M_2 (where M_1 and M_2 are the masses of the donor and the accretor, respectively) exceeds a critical value q_c (Hjellming & Webbink 1987). Webbink (1988) estimates this critical mass ratio, for $M_c \geq 0.2$, as

$$q_c = 0.362 + \frac{1}{3(1 - M_c/M_1)}, \tag{7}$$

where M_c is the mass contained in the donor star's core and M_1 is the mass of the donor star. Dynamically unstable mass transfer is expected to lead to the formation of a common envelope (CE), which consists mainly of material from the envelope of the donor star. Embedded in this envelope are the dense, small core of the mass donor and the more or less unaffected companion star. Owing to frictional drag with the envelope, the orbit of the embedded binary decays. A large fraction of the orbital energy that is released in this spiral-in process is deposited in the envelope (Livio & Soker 1988), and the envelope may be ejected when the total deposited orbital energy, $\alpha_{CE}\Delta E_{orb}$, is larger than the envelope binding energy E_{env}, i.e.

$$\alpha_{CE}\Delta E_{orb} \geq E_{gr} - \alpha_{th} E_{th}, \tag{8}$$

where

$$\Delta E_{orb} \simeq \frac{GM_c M_2}{2a_f} - \frac{G(M_c + M_e)M_2}{2a_i}$$

is the orbital energy released in the orbital contraction, and E_{gr} and E_{th} are the envelope gravitational energy and envelope thermal energy at the beginning of RLOF; here, M_c, M_e and M_2 are the core mass and envelope mass of the primary, and the mass of the secondary, respectively, and a_i and a_f are the initial and final separations, respectively. In equation (8) we have introduced an efficiency parameter α_{CE} to parametrize the uncertainties of the CE ejection process. We take α_{CE} to be 0.3 or 1.0. Note that our definition of α_{CE} differs substantially from the definition by Iben & Tutukov (1984a) (see Section 6.10). CE ejection is expected to generate a high-density contrast for first giant branch stars (FGB) and a mild density contrast for AGB stars (Livio & Soker 1988) and thus can account for a variety of PN shapes. All of the PNe produced in this way have close binary nuclei.

If the orbital energy released during the spiral-in is not sufficient to eject the common envelope, the two immersed binary components will merge completely and lead to a single, coalesced star – FK Com stars (Bopp & Stencel 1981) and V Hya (Kahane, Maizels & Jura 1988) may be such merger products. The merged system will initially be rotating near breakup, and mass loss from the star will be strongly enhanced in the orbital plane, producing a disc-like outflow in the process and ultimately a bipolar PN with a single-star nucleus. We expect to form a bipolar PN from most merged binaries, even if the star is no longer rapidly rotating at the time of PN ejection, because the disc-like structure formed during or just after the merger phase will provide an equatorial constraint which will shape the subsequent mass loss into a bipolar flow.

3.4 Cataclysmic variables, double degenerates and Type Ia supernovae

A short-period binary system, consisting of a white dwarf (WD) and a main-sequence (MS) companion, which survives the CE phase, may later form a semidetached system because of orbital angular momentum losses due to magnetic braking (Eggleton 1976; Verbunt & Zwaan 1981) and gravitational wave radiation (e.g. Landau & Lifshitz 1962). According to Kolb (1993), magnetic braking requires that the MS companion has a mass greater than $\sim 0.37\ M_\odot$. If mass transfer in the resulting semidetached system is stable, a cataclysmic variable (CV) is formed. In order to determine which systems actually become CVs within the age of the Galaxy, we adopt the formalism devised by de Kool (1992) for our simulations.

Double-degenerate systems (DDs), i.e. binaries consisting of two degenerate stars, are formed after one or two CE ejections. Subsequently, the orbital angular momentum loss due to gravitational radiation may lead to the merger of the DD system. The wider DDs that have not already coalesced in the past can in principle be observed, although only two are currently known (Saffer, Liebert & Olszewski 1988; Bragaglia, Renzini & Bergeron 1993). A Type Ia supernova (SN Ia) explosion may happen as a result of a DD merger if the total mass is larger than the Chandrasekhar limit (Sparks

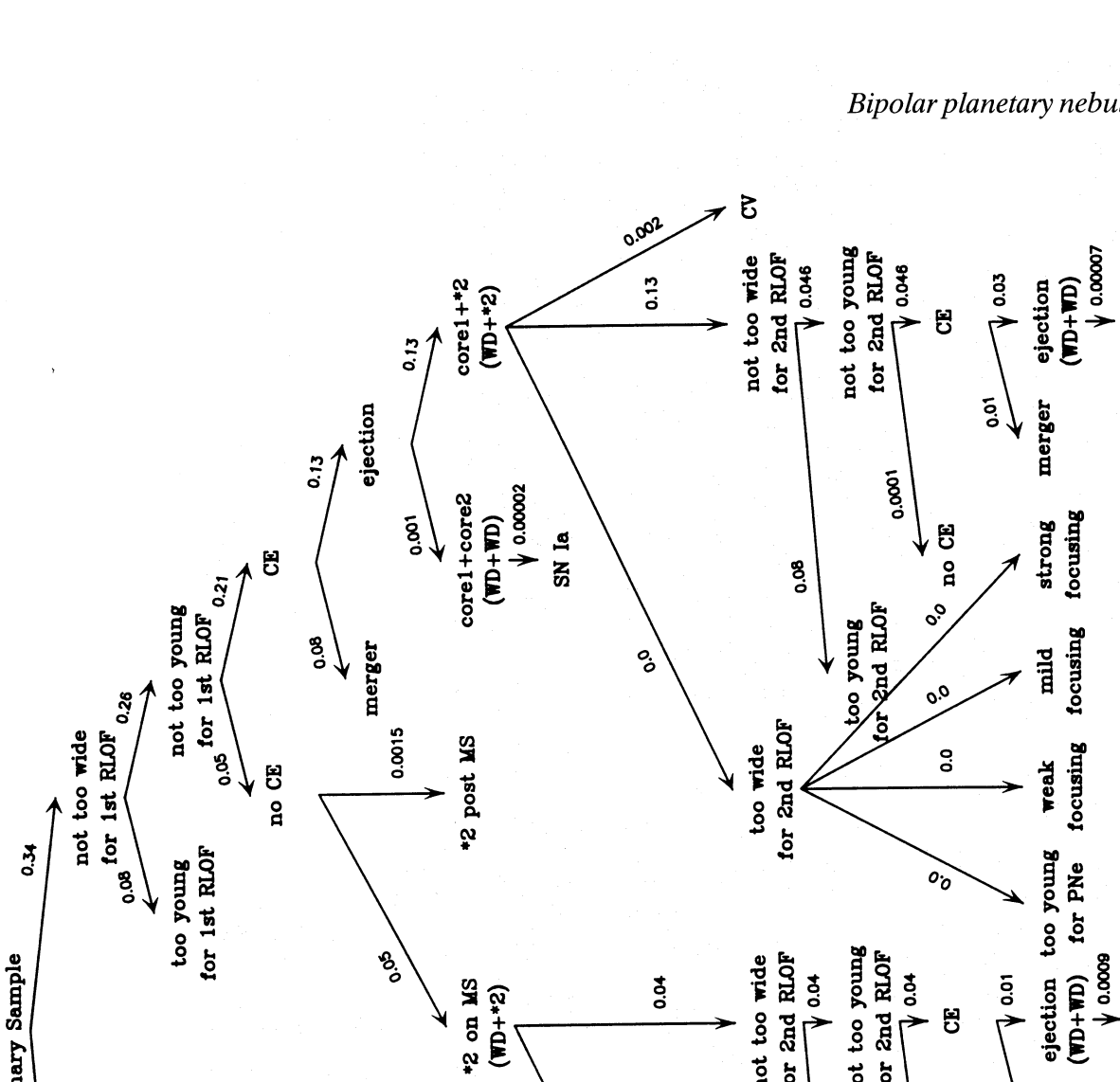

Figure 2. Flow chart for the Monte Carlo simulations. RLOF stands for Roche lobe overflow, CE for common envelope, MS for main sequence, WD for white dwarf, ∗1 for star 1 (primary), and ∗2 for star 2 (secondary). The figures give the percentages for each evolutionary channel in simulation 6. See text for further explanations.

& Stecher 1974; Iben & Tutukov 1984a,b; Webbink & Iben 1987; see also, however, Nomoto & Iben 1985).

3.5 Binary evolution flow chart

A schematic flow chart for the evolution of a collection of binaries is shown in Fig. 2. Sample binaries are generated on the zero-age main sequence (ZAMS) with specified distributions for the star formation rate, primary masses, mass ratios, and orbital separations (see Section 4). In the following description, expressions in square brackets refer to the corresponding channels in Fig. 2.

If the initial separation of a binary system is too large, its components will never fill their Roche lobes, and the system will never experience RLOF [too wide for 1st RLOF]. If the evolution time from the ZAMS to PN ejection is greater than the age of the population [∗1 too young for PNe], the detached system will not produce a PN. If the evolution time is shorter, a PN is produced and influenced by gravitational focusing according to equation (6) [∗1 weak focusing, ∗1 mild focusing, ∗1 strong focusing]. The subsequent evolution of the secondary is treated similarly [∗2 too young for PNe, ∗2 weak focusing, ∗2 mild focusing, ∗2 strong focusing].

If the initial separation of a binary system is sufficiently small, the system will experience RLOF [not too wide for 1st RLOF], unless the evolution time from the ZAMS to RLOF is greater than the age of the population [too young for 1st RLOF]. If RLOF occurs [not too young for 1st RLOF], mass transfer can be stable [no CE] or unstable [CE]. In the case of stable RLOF transfer, the envelope of the primary is transferred to the secondary, leaving a helium star (van der Linden 1987) and finally a helium WD or carbon–oxygen WD (e.g. Paczyński 1971). If the secondary is a main-sequence star at the beginning of RLOF, it is assumed that it is rejuvenated as a more massive star and is subsequently treated like a star born at the time of RLOF [WD + ∗2, MS].

In the case of dynamically unstable mass transfer, the first phase of RLOF will result in the formation of a CE and a spiral-in phase. If, in the spiral-in process, not enough energy is deposited in the envelope to eject the CE, the system merges to form a single star [merger]. If enough energy is deposited, the CE is ejected [ejection]. Very occasionally, a CE phase results from the mass transfer between two red giants, and the CE will engulf two degenerate cores. In this case, CE ejection will produce a DD system [WD + WD]. Otherwise, CE ejection leaves a binary system with only one WD component [WD + ∗2], and the further evolution can lead to a second phase of RLOF, subject to the same possibilities as the first phase of RLOF (in this case, CE ejection will leave a DD system).

The evolution of a binary system containing a WD and a normal star may lead to the formation of a CV [CV], and that of a DD system may lead to a Type Ia SN [SN Ia].

4 MONTE CARLO SIMULATIONS

To estimate the importance of the various evolutionary channels for the production of bipolar PNe, we have performed a series of detailed Monte Carlo simulations. In each simulation, we follow the evolution of 10^6 sample binaries according to our grid of stellar models and the evolutionary channels in Fig. 2. In addition, the simulations require as input the star formation rate (SFR), the initial mass function (IMF) of the primary, the initial mass-ratio distribution and the distribution of initial orbital separations. Many of these distributions are only poorly known observationally, and some of them are even controversial (see, for example, Abt & Levy 1976, 1978; Kraicheva et al. 1978, 1979; Morbey & Griffin 1987; Duquennoy & Mayor 1990; Mazeh et al. 1992; Goldberg & Mazeh 1994). We make the following assumptions.

(i) The SFR is taken to be constant over the last 15 Gyr.

(ii) A simple approximation to the IMF of Miller & Scalo (1979) is used; the primary mass is generated with the formula devised by Eggleton, Fitchett & Tout (1989)

$$M_1 = \frac{0.19X}{(1-X)^{0.75} + 0.032(1-X)^{0.25}}, \tag{9}$$

where X is a random number between 0 and 1. The adopted ranges of primary masses are 0.8 $M_\odot$ to 8.0 $M_\odot$ for Pop I, and 0.8 $M_\odot$ to 7.0 $M_\odot$ for Pop II.

(iii) The mass-ratio distribution of binary systems is quite controversial. We therefore consider three different distributions:

(a) a constant mass-ratio distribution

$$n(q) = \text{const.}, \qquad 0 \le q \le 1, \tag{10}$$

where $q = M_2/M_1$.

(b) a distribution where both components are chosen randomly and independently from the same IMF (i.e. equation 9).

(c) a distribution rising towards equal mass ratio

$$n(q) = 2q, \qquad 0 \le q \le 1. \tag{11}$$

(iv) We assume that all stars are members of binary systems and that the distribution of separations is constant in $\log a$ for wide binaries and falls off smoothly at close separations:

$$an(a) = \begin{cases} \alpha_{\rm sep}(a/a_0)^n & a \le a_0; \\ \alpha_{\rm sep} & a_0 < a < a_1, \end{cases} \tag{12}$$

where $\alpha_{\rm sep} \approx 0.070$, $a_0 = 10\ R_\odot$, $a_1 = 5.75 \times 10^6\ R_\odot = 0.13$ pc and $n \approx 1.2$. This distribution implies that there are equal numbers of wide binary systems per logarithmic interval, and that approximately 50 per cent of stellar systems are binary systems with orbital periods less than 100 yr.

5 RESULTS

To test the results of our simulations, we compared them with those of the two earlier, related studies by de Kool (1992) and Yungelson et al. (1993). Generally, we found that, with the same assumptions (initial distributions, etc.), our results are in good agreement with both studies; i.e. we obtain similar birth rates, mass distributions and orbital period distributions for various types of binaries. There are substantial differences in the results, however, when we use our somewhat different initial distributions, treatment of the CE phase, etc.; these will be further discussed in Section 6.10.

Table 1. Percentages for different evolutionary channels of PN formation. The simulations assume that 50 per cent of all stellar systems are binaries with periods less than 100 yr. The second and third columns give the values of the common-envelope (CE) parameters α_{CE} and α_{th}. The fourth column specifies the adopted mass-ratio distribution (a: constant distribution; b: uncorrelated component masses; c: rising towards unit mass ratio). FGB stands for first giant branch, AGB for asymptotic giant branch, and m_i for the initial primary mass. All simulations in this table assume an age of 15 Gyr and use the HPE initial–final mass relation (Han et al. 1994).

Model Set	α_{CE}	α_{th}	$n(q)$	Weak Focusing	Mild Focusing	Strong Focusing	CE Merger	CE Ejection (FGB)	CE Ejection (AGB)	Bipolar PNe	
1	0.3	0.0	a	61.04	9.66	3.24	21.35	2.55	2.16	38.96	
				62.05	8.69	2.23	20.96	3.94	2.14	37.95	$0.8\,M_\odot < m_i < 2\,M_\odot$
				59.61	10.89	4.23	22.44	0.00	2.83	40.39	$2\,M_\odot \leq m_i \leq 4\,M_\odot$
				58.04	12.99	7.64	21.00	0.00	0.34	41.96	$4\,M_\odot < m_i < 8\,M_\odot$
2	0.3	0.5	a	60.62	9.62	3.24	19.55	3.96	3.02	39.38	
				61.40	8.74	2.23	19.38	6.10	2.15	38.60	$0.8\,M_\odot < m_i < 2\,M_\odot$
				59.51	10.78	4.19	20.02	0.05	5.44	40.49	$2\,M_\odot \leq m_i \leq 4\,M_\odot$
				58.23	12.53	7.65	19.36	0.00	2.24	41.77	$4\,M_\odot < m_i < 8\,M_\odot$
3	0.3	1.0	a	60.04	9.50	3.18	16.16	6.95	4.18	39.96	
				60.62	8.62	2.18	16.05	10.39	2.14	39.38	$0.8\,M_\odot < m_i < 2\,M_\odot$
				59.18	10.60	4.18	16.83	0.65	8.56	40.82	$2\,M_\odot \leq m_i \leq 4\,M_\odot$
				58.30	12.72	7.52	15.05	0.08	6.34	41.70	$4\,M_\odot < m_i < 8\,M_\odot$
4	1.0	0.0	a	60.05	9.50	3.17	15.68	7.27	4.33	39.95	
				60.54	8.64	2.16	15.60	10.90	2.16	39.46	$0.8\,M_\odot < m_i < 2\,M_\odot$
				59.26	10.52	4.23	16.40	0.60	8.99	40.74	$2\,M_\odot \leq m_i \leq 4\,M_\odot$
				58.73	12.83	7.42	14.22	0.15	6.64	41.27	$4\,M_\odot < m_i < 8\,M_\odot$
5	1.0	0.5	a	59.61	9.46	3.16	13.74	9.19	4.83	40.39	
				60.02	8.53	2.17	13.66	13.46	2.15	39.98	$0.8\,M_\odot < m_i < 2\,M_\odot$
				59.00	10.61	4.22	14.53	1.38	10.27	41.00	$2\,M_\odot \leq m_i \leq 4\,M_\odot$
				58.41	12.95	7.30	12.02	0.70	8.62	41.59	$4\,M_\odot < m_i < 8\,M_\odot$
6	1.0	1.0	a	59.16	9.36	3.17	11.14	11.72	5.45	40.84	
				59.63	8.39	2.17	11.17	16.56	2.09	40.37	$0.8\,M_\odot < m_i < 2\,M_\odot$
				58.35	10.65	4.17	11.96	2.71	12.17	41.65	$2\,M_\odot \leq m_i \leq 4\,M_\odot$
				58.04	12.74	7.63	8.63	2.23	10.71	41.96	$4\,M_\odot < m_i < 8\,M_\odot$
7	1.0	1.0	c	57.40	12.10	3.07	10.23	11.79	5.41	42.60	
				58.31	11.41	2.33	10.30	16.46	1.19	41.69	$0.8\,M_\odot < m_i < 2\,M_\odot$
				57.00	13.32	4.27	10.79	2.92	11.70	43.00	$2\,M_\odot \leq m_i \leq 4\,M_\odot$
				51.63	13.79	5.25	8.00	2.05	19.28	48.37	$4\,M_\odot < m_i < 8\,M_\odot$
8	0.3	0.0	b	65.68	2.19	0.52	27.17	2.37	2.06	34.32	
				64.45	2.52	0.62	26.13	3.72	2.55	35.55	$0.8\,M_\odot < m_i < 2\,M_\odot$
				65.91	1.65	0.35	30.48	0.00	1.61	34.09	$2\,M_\odot \leq m_i \leq 4\,M_\odot$
				73.18	1.48	0.32	24.96	0.00	0.06	26.82	$4\,M_\odot < m_i < 8\,M_\odot$
9	0.3	0.5	b	65.59	2.19	0.55	24.80	3.96	2.91	34.41	
				64.34	2.49	0.65	23.62	6.20	2.71	35.66	$0.8\,M_\odot < m_i < 2\,M_\odot$
				65.97	1.67	0.38	27.62	0.03	4.32	34.03	$2\,M_\odot \leq m_i \leq 4\,M_\odot$
				72.78	1.63	0.34	24.87	0.00	0.39	27.22	$4\,M_\odot < m_i < 8\,M_\odot$
10	0.3	1.0	b	65.35	2.23	0.56	20.99	6.72	4.15	34.65	
				64.01	2.55	0.68	19.63	10.36	2.78	35.99	$0.8\,M_\odot < m_i < 2\,M_\odot$
				65.61	1.72	0.36	23.62	0.39	8.31	34.39	$2\,M_\odot \leq m_i \leq 4\,M_\odot$
				73.55	1.50	0.32	22.76	0.02	1.85	26.45	$4\,M_\odot < m_i < 8\,M_\odot$
11	1.0	0.0	b	65.46	2.23	0.57	20.55	7.09	4.10	34.54	
				64.13	2.53	0.67	19.04	10.93	2.70	35.87	$0.8\,M_\odot < m_i < 2\,M_\odot$
				65.89	1.73	0.41	23.18	0.41	8.38	34.11	$2\,M_\odot \leq m_i \leq 4\,M_\odot$
				73.01	1.65	0.33	23.37	0.07	1.58	26.99	$4\,M_\odot < m_i < 8\,M_\odot$
12	1.0	0.5	b	65.26	2.23	0.58	18.31	8.83	4.78	34.74	
				63.86	2.51	0.67	16.83	13.40	2.73	36.14	$0.8\,M_\odot < m_i < 2\,M_\odot$
				65.89	1.77	0.42	20.64	0.95	10.33	34.11	$2\,M_\odot \leq m_i \leq 4\,M_\odot$
				72.74	1.68	0.38	21.78	0.25	3.16	27.26	$4\,M_\odot < m_i < 8\,M_\odot$
13	1.0	1.0	b	65.12	2.24	0.57	15.27	11.03	5.77	34.88	
				63.73	2.55	0.70	13.92	16.37	2.72	36.27	$0.8\,M_\odot < m_i < 2\,M_\odot$
				65.55	1.72	0.36	17.48	1.97	12.91	34.45	$2\,M_\odot \leq m_i \leq 4\,M_\odot$
				73.13	1.66	0.28	18.07	0.65	6.22	26.87	$4\,M_\odot < m_i < 8\,M_\odot$

Altogether, we performed 13 sets of calculations with different values for the CE parameters α_{CE} and α_{th} and the different mass-ratio distributions. The results of these simulations are shown in Table 1, where we give the percentages of PNe formed via the different evolutionary channels; we also list the percentages for different initial mass ranges for the primary separately ($0.8\,M_\odot \le m_i < 2\,M_\odot$, $2\,M_\odot \le m_i \le 4\,M_\odot$, and $4\,M_\odot < m_i \le 8\,M_\odot$). In Table 2, we give the frequency for each evolutionary channel in our Galaxy, assuming that one binary with $M_1 \ge 0.8\ M_\odot$ is formed annually in our Galaxy (e.g. Yungelson et al. 1993; Iben & Tutukov 1984a). An effective Galactic volume of 5×10^{11} pc^3 gives a birth rate for WDs (including WDs in binaries) of 2×10^{-12} pc^{-3} yr^{-1}, consistent with observations (Weidemann 1990); to convert the figures in Table 2 into birth rates in pc^{-3} yr^{-1}, one has to multiply them by 2×10^{-12} pc^{-3}.

We also performed simulations to investigate the effects of metallicity, of the initial–final mass relation, and the age of the population. The results of these calculations are presented in Tables 3 and 4.

6 DISCUSSION

6.1 The importance of individual evolutionary channels

The most important result of the present study is that binary interactions should affect the structure of some 34 to 43 per cent of all PNe (see Table 1, which assumes that 50 per cent of all binaries have periods less than 100 yr; for a different assumed fraction, the answers should be rescaled accordingly). The formation of 3 to 15 per cent PNe is affected by mild and strong focusing in detached binary systems. Common-envelope evolution is the most important channel for the formation of bipolar PNe, accounting for the formation of 27 to 32 per cent of PNe. CE ejection and coalescence during the CE phase are of similar importance. CE ejection is expected to produce up to 17 per cent of PNe, while the merger scenario can account for more than 10 per cent of asymmetric PNe.

6.2 The role of the initial primary mass

In Table 1 we list the percentages for the various evolutionary channels separately for different initial primary mass ranges ($0.8\,M_\odot < m_i < 2\,M_\odot$, $2\,M_\odot \le m_i \le 4\,M_\odot$, $4\,M_\odot < m_i < 8\,M_\odot$). Inspection of the table shows that, for a constant mass-ratio distribution (simulations 1 to 6), a bipolar PN is slightly more likely to be formed from a binary with a higher initial primary mass. This effect is mainly a consequence of the constant initial mass-ratio distribution, since, in this case, a more massive primary tends to have a more massive secondary and thus is more likely to produce a bipolar PN via mild gravitational focusing or strong gravitational focusing (see equation 6).

If the masses of the binary components are chosen independently (simulations 8 to 13), however, a more massive binary is less likely to produce a bipolar PN. The reason for this slightly paradoxical result is that we assume that stars that fill their Roche lobes in the Hertzsprung gap experience stable mass transfer rather than a common-envelope phase; since these stars do not subsequently eject PNe, and since the Hertzsprung gap increases with increasing mass, the fraction of bipolar PNe decreases; thus the main effect of binary interaction in these cases is to prevent the ejection of a PN altogether.

Finally, if the mass-ratio distribution is rising towards equal mass ratio (simulation 7), the fraction of bipolar PNe

Table 2. Birth rates (frequencies) for various types of systems (events) per year in our Galaxy for the simulations in Table 1. The figures assume that one binary with $M_1 \ge 0.8\ M_\odot$ is formed annually in our Galaxy. CV stands for cataclysmic variable, DD for double-degenerate systems. The SN Ia frequency assumes that Type Ia supernovae result from the merger of two CO white dwarfs with a total mass larger than the Chandrasekhar mass. The last column gives the frequency for the merger of carbon–oxygen white dwarfs with helium white dwarfs. The birth rates/frequencies can be approximately converted into local birth rates/frequencies (in units of pc^{-3} yr^{-1}) by multiplying them by a factor of 2×10^{-12} pc^{-3}.

Model Set	α_{CE}	α_{th}	$n(q)$	Weak Focusing	Mild Focusing	Strong Focusing	CE Merger	CE Ejection (FGB)	CE Ejection (AGB)	Bipolar PNe	CV	DD	DD Merger	SN Ia	CO + He WD Merger
1	0.3	0.0	a	0.583	0.092	0.031	0.204	0.024	0.021	0.423	0.0021	0.0006	0.0006	0.0001	0.0008
2	0.3	0.5	a	0.583	0.092	0.031	0.188	0.038	0.029	0.429	0.0019	0.0035	0.0035	0.0010	0.0023
3	0.3	1.0	a	0.583	0.092	0.031	0.157	0.067	0.041	0.439	0.0016	0.0167	0.0119	0.0016	0.0043
4	1.0	0.0	a	0.583	0.092	0.031	0.152	0.071	0.042	0.439	0.0025	0.0150	0.0145	0.0020	0.0057
5	1.0	0.5	a	0.582	0.092	0.031	0.134	0.090	0.047	0.445	0.0023	0.0242	0.0201	0.0016	0.0067
6	1.0	1.0	a	0.581	0.092	0.031	0.109	0.115	0.054	0.452	0.0019	0.0367	0.0190	0.0009	0.0046
7	1.0	1.0	c	0.612	0.129	0.033	0.109	0.126	0.058	0.506	0.0004	0.0536	0.0261	0.0010	0.0062
8	0.3	0.0	b	0.520	0.017	0.004	0.215	0.019	0.016	0.317	0.0068	0.0001	0.0001	0.0000	0.0001
9	0.3	0.5	b	0.519	0.017	0.004	0.196	0.031	0.023	0.318	0.0074	0.0005	0.0005	0.0001	0.0002
10	0.3	1.0	b	0.519	0.018	0.004	0.167	0.053	0.033	0.321	0.0065	0.0027	0.0020	0.0002	0.0005
11	1.0	0.0	b	0.519	0.018	0.004	0.163	0.056	0.032	0.319	0.0094	0.0025	0.0024	0.0003	0.0007
12	1.0	0.5	b	0.519	0.018	0.005	0.146	0.070	0.038	0.322	0.0090	0.0043	0.0037	0.0003	0.0010
13	1.0	1.0	b	0.518	0.018	0.005	0.121	0.088	0.046	0.323	0.0080	0.0066	0.0038	0.0002	0.0007

Table 3. Similar to Table 1, for populations of different ages and metallicities, and different assumed initial–final mass relations (as indicated in the right column). HPE stands for the Han et al. (1994) initial–final mass relation, YTL for the fit by Yungelson et al. (1993) to the Weidemann & Koester (1983) relation, and IT for the Iben & Tutukov (1984a) relation.

Model Set	α_{CE}	α_{th}	$n(q)$	Weak Focusing	Mild Focusing	Strong Focusing	CE Merger	CE Ejection (FGB)	CE Ejection (AGB)	Bipolar PNe	
14	1.0	1.0	a	58.11	10.16	2.98	12.02	8.18	8.56	41.89	*Pop I, 5 Gyr, HPE*
				58.32	9.37	2.55	12.89	14.75	2.11	41.68	$0.8\,M_\odot < m_i < 2\,M_\odot$
				58.83	10.69	3.37	12.04	2.79	12.27	41.17	$2\,M_\odot \leq m_i \leq 4\,M_\odot$
				55.35	11.17	3.27	9.10	2.28	18.84	44.65	$4\,M_\odot < m_i < 8\,M_\odot$
15	1.0	1.0	a	58.45	10.17	3.83	11.95	8.08	7.52	41.55	*Pop I, 5 Gyr, YTL*
				58.26	9.03	2.51	12.97	14.67	2.56	41.74	$0.8\,M_\odot < m_i < 2\,M_\odot$
				58.79	10.61	4.09	11.82	2.64	12.06	41.21	$2\,M_\odot \leq m_i \leq 4\,M_\odot$
				58.08	12.65	7.41	8.97	2.32	10.58	41.92	$4\,M_\odot < m_i < 8\,M_\odot$
16	1.0	1.0	a	57.75	9.10	1.75	12.06	8.51	10.84	42.25	*Pop I, 5 Gyr, IT*
				58.34	8.82	1.57	12.83	15.51	2.93	41.66	$0.8\,M_\odot < m_i < 2\,M_\odot$
				58.06	9.21	1.71	12.18	2.75	16.09	41.94	$2\,M_\odot \leq m_i \leq 4\,M_\odot$
				54.89	9.67	2.45	9.20	2.33	21.45	45.11	$4\,M_\odot < m_i < 8\,M_\odot$
17	1.0	1.0	a	59.16	9.60	2.57	11.19	11.78	5.71	40.84	*Pop I, 15 Gyr, HPE*
				59.80	9.04	2.18	11.08	16.58	1.32	40.20	$0.8\,M_\odot < m_i < 2\,M_\odot$
				58.68	10.55	3.26	12.12	2.87	12.52	41.32	$2\,M_\odot \leq m_i \leq 4\,M_\odot$
				55.77	11.01	3.41	9.27	2.24	18.30	44.23	$4\,M_\odot < m_i < 8\,M_\odot$
18	1.0	1.0	a	59.17	9.40	3.15	11.07	11.73	5.47	40.83	*Pop I, 15 Gyr, YTL*
				59.47	8.50	2.18	11.13	16.63	2.09	40.53	$0.8\,M_\odot < m_i < 2\,M_\odot$
				58.53	10.49	4.17	11.77	2.68	12.36	41.47	$2\,M_\odot \leq m_i \leq 4\,M_\odot$
				58.84	12.85	7.23	8.67	2.13	10.29	41.16	$4\,M_\odot < m_i < 8\,M_\odot$
19	1.0	1.0	a	58.80	9.01	1.64	11.25	12.17	7.13	41.20	*Pop I, 15 Gyr, IT*
				59.64	8.75	1.53	11.13	17.13	1.82	40.36	$0.8\,M_\odot < m_i < 2\,M_\odot$
				57.97	9.35	1.72	12.29	2.85	15.83	42.03	$2\,M_\odot \leq m_i \leq 4\,M_\odot$
				54.92	9.94	2.27	9.14	2.28	21.45	45.08	$4\,M_\odot < m_i < 8\,M_\odot$
20	1.0	1.0	a	60.39	10.09	2.78	7.43	8.47	10.84	39.61	*Pop II, 5 Gyr, HPE*
				61.56	9.61	2.42	7.93	13.18	5.31	38.44	$0.8\,M_\odot < m_i < 2\,M_\odot$
				59.49	10.70	3.31	7.29	2.07	17.15	40.51	$2\,M_\odot \leq m_i \leq 4\,M_\odot$
				56.10	11.10	3.28	4.79	0.31	24.41	43.90	$4\,M_\odot < m_i < 7\,M_\odot$
21	1.0	1.0	a	62.61	12.56	10.26	6.42	6.76	1.38	37.39	*Pop II, 5 Gyr, YTL*
				61.50	11.14	6.99	7.73	10.82	1.83	38.50	$0.8\,M_\odot < m_i < 2\,M_\odot$
				63.01	14.53	15.42	5.10	1.26	0.68	36.99	$2\,M_\odot \leq m_i \leq 4\,M_\odot$
				68.11	14.76	13.13	2.81	0.22	0.97	31.89	$4\,M_\odot < m_i < 7\,M_\odot$
22	1.0	1.0	a	62.07	11.98	7.42	6.85	7.36	4.32	37.93	*Pop II, 5 Gyr, IT*
				61.90	11.02	5.40	7.77	11.73	2.18	38.10	$0.8\,M_\odot < m_i < 2\,M_\odot$
				61.79	13.20	10.80	6.03	1.42	6.76	38.21	$2\,M_\odot \leq m_i \leq 4\,M_\odot$
				64.12	13.83	8.57	3.84	0.23	9.40	35.88	$4\,M_\odot < m_i < 7\,M_\odot$
23	1.0	1.0	a	61.26	9.51	2.41	7.22	11.91	7.69	38.74	*Pop II, 15 Gyr, HPE*
				62.08	9.13	2.12	7.42	15.53	3.72	37.92	$0.8\,M_\odot < m_i < 2\,M_\odot$
				59.65	10.56	3.22	7.18	2.05	17.35	40.35	$2\,M_\odot \leq m_i \leq 4\,M_\odot$
				56.52	10.64	3.28	5.01	0.30	24.25	43.48	$4\,M_\odot < m_i < 7\,M_\odot$
24	1.0	1.0	a	62.33	11.38	7.95	6.65	10.24	1.46	37.67	*Pop II, 15 Gyr, YTL*
				61.67	10.20	5.46	7.38	13.58	1.70	38.33	$0.8\,M_\odot < m_i < 2\,M_\odot$
				62.83	14.67	15.38	5.15	1.29	0.69	37.17	$2\,M_\odot \leq m_i \leq 4\,M_\odot$
				68.57	14.57	12.79	2.82	0.19	1.06	31.43	$4\,M_\odot < m_i < 7\,M_\odot$
25	1.0	1.0	a	62.11	11.32	6.03	6.82	10.75	2.96	37.89	*Pop II, 15 Gyr, IT*
				62.03	10.58	4.59	7.27	14.13	1.40	37.97	$0.8\,M_\odot < m_i < 2\,M_\odot$
				61.86	13.33	10.57	6.08	1.52	6.65	38.14	$2\,M_\odot \leq m_i \leq 4\,M_\odot$
				64.01	13.74	8.43	3.78	0.31	9.73	35.99	$4\,M_\odot < m_i < 7\,M_\odot$

increases quite drastically with increasing primary mass (from 42 to 48 per cent). This suggests that the effect, claimed by Zuckerman & Gatley (1988), that bipolar PNe are more likely to be associated with more massive systems, can be best explained by binary interactions if the mass-ratio distribution is rising.

6.3 The role of α_{CE} and α_{th}

As expected, the coefficients α_{CE} and α_{th} strongly influence the outcome of the CE phase (see the columns headed 'CE' in Tables 1 and 2), in particular the ratio of CE mergers to CE ejections. If more orbital energy is deposited in the

Table 4. Similar to Table 2, for the simulations in Table 3.

Model Set	α_{CE}	α_{th}	$n(q)$	Weak Focusing	Mild Focusing	Strong Focusing	CE Merger	CE Ejection (FGB)	CE Ejection (AGB)	Bipolar PNe	CV	DD	DD Merger	SN Ia	CO + He WD Merger	
14	1.0	1.0	a	0.362	0.063	0.019	0.075	0.051	0.053	0.307	0.0009	0.0252	0.0096	0.0006	0.0034	*Pop I, 5 Gyr, HPE*
15	1.0	1.0	a	0.366	0.064	0.024	0.075	0.051	0.047	0.305	0.0009	0.0216	0.0094	0.0006	0.0032	*Pop I, 5 Gyr, YTL*
16	1.0	1.0	a	0.361	0.057	0.011	0.075	0.053	0.068	0.309	0.0010	0.0303	0.0098	0.0007	0.0035	*Pop I, 5 Gyr, IT*
17	1.0	1.0	a	0.583	0.095	0.025	0.110	0.116	0.056	0.452	0.0021	0.0401	0.0198	0.0010	0.0052	*Pop I, 15 Gyr, HPE*
18	1.0	1.0	a	0.582	0.093	0.031	0.109	0.115	0.054	0.452	0.0020	0.0368	0.0189	0.0009	0.0047	*Pop I, 15 Gyr, YTL*
19	1.0	1.0	a	0.578	0.089	0.016	0.111	0.120	0.070	0.455	0.0021	0.0463	0.0194	0.0010	0.0050	*Pop I, 15 Gyr, IT*
20	1.0	1.0	a	0.478	0.080	0.022	0.059	0.067	0.086	0.395	0.0016	0.0474	0.0160	0.0035	0.0063	*Pop II, 5 Gyr, HPE*
21	1.0	1.0	a	0.506	0.102	0.083	0.052	0.055	0.011	0.380	0.0003	0.0109	0.0067	0.0004	0.0011	*Pop II, 5 Gyr, YTL*
22	1.0	1.0	a	0.496	0.096	0.059	0.055	0.059	0.035	0.382	0.0009	0.0229	0.0104	0.0013	0.0037	*Pop II, 5 Gyr, IT*
23	1.0	1.0	a	0.760	0.118	0.030	0.090	0.148	0.095	0.579	0.0035	0.0701	0.0308	0.0045	0.0092	*Pop II, 15 Gyr, HPE*
24	1.0	1.0	a	0.784	0.143	0.100	0.084	0.129	0.018	0.567	0.0014	0.0269	0.0176	0.0004	0.0017	*Pop II, 15 Gyr, YTL*
25	1.0	1.0	a	0.779	0.142	0.076	0.086	0.135	0.037	0.569	0.0023	0.0400	0.0230	0.0017	0.0059	*Pop II, 15 Gyr, IT*

envelope, the number of mergers is reduced and the number of CE ejections is increased. The envelope thermal energy contribution to the total envelope binding energy has a similar effect to α_{CE}; an increase in α_{th} from 0 to 1 is roughly equivalent to an increase of α_{CE} from 0.3 to 1. We also note from Table 1 that FGB envelope ejections are more sensitive to α_{CE} and α_{th} than AGB envelope ejections.

Theoretically, the values of α_{CE} and α_{th} are very uncertain. Unless there is some other energy source [see the discussion in Livio (1994)], the largest possible value of both α_{CE} and α_{th} is 1 [note that our α_{CE} is very different from the identically named parameter of Livio & Soker (1988); see Section 6.10].

6.4 The role of the mass-ratio distribution

Compared with the constant mass-ratio distribution, the mass-ratio distribution for uncorrelated masses peaks at lower q. Consequently, the secondary is more likely to be less massive; this leads to a sharp decrease of systems with mild or strong gravitational focusing, to more merger cases, and to fewer common-envelope ejections. Hence the number of bipolar PNe and PNe with close binary cores in general is reduced.

6.5 The distribution of masses of PN nuclei

Fig. 3 displays the distribution of masses of PN nuclei for a few representative simulations (simulations 1, 4, 6, 7 and 13). The distributions are very similar in all cases and peak sharply at 0.59 ± 0.02 $M_\odot$. Note that the shape of the peak is highly non-Gaussian; the quoted range is defined to include half of all PN nuclei.

6.6 Close white dwarf binaries

If, as a result of a CE phase, the envelope is ejected, the resulting system is a short-period binary containing at least one degenerate dwarf. Fig. 4 shows the primary (WD) mass distribution, the mass-ratio distribution, and the period distribution for binary systems that survived the CE phase for simulations 4 and 6. Unlike simulation 4, simulation 6 takes into account the thermal energy term in the envelope binding energy calculation ($\alpha_{th} = 1$). Therefore the orbital periods in simulation 6 tend to be longer than in simulation 4, extending up to ~1000 d. This is very different from the results of the studies by de Kool (1992) and Yungelson et al. (1993), who use simple, analytical homology relations for the binding energy. As was found by Han et al. (1994b), the binding energy of evolved stars decreases significantly below the value obtained from a homology relation and eventually becomes positive. At this point, the envelope is presumably ejected as a PN. If a binary experiences a CE phase when the envelope binding energy of the component that has filled its Roche lobe is already greatly reduced, very little orbital shrinkage is required to eject the common envelope. Therefore the final binary will have a relatively long orbital period. This could help to explain the formation of certain symbiotic binaries which should have experienced a CE phase but still have relatively long periods (several 100 d).

6.7 CV formation

Some of the close white dwarf binaries will form CVs, i.e. systems in which a main-sequence star that fills its Roche lobe transfers mass to a white dwarf companion, if the orbit shrinks sufficiently due to gravitational radiation and magnetic braking before the main-sequence component had time to evolve off the main sequence. Fig. 5 shows the expected WD mass distribution and the orbital period distribution in CVs for simulations 4 and 6. Mass transfer is more likely to be stable in a semidetached binary system when the accreting WD is more massive (de Kool 1992), and close binaries with higher WD masses are more easily formed in simulation 6 than in simulation 4. Hence the average mass of WDs above the mass distribution gap at 0.48–0.55 $M_\odot$ is 0.78 $M_\odot$ for simulation 4 and 0.82 $M_\odot$ for simulation 6 [simulation 4 is similar to model 1 of de Kool (1992)].

The CV birth rate in our simulations is $(0.08\text{–}2) \times 10^{-14}$ pc^{-3} yr^{-1} (see Table 2) and is quite sensitive to the mass-ratio distribution. For the mass-ratio distribution of uncorre-

lated component masses, the secondary tends to be less massive, and the orbital period of the WD binary after the CE phase is, on average, shorter. It therefore takes less time for the system to reach the phase of RLOF. Moreover, RLOF is more likely to be dynamically and thermally stable for a WD binary with a less massive secondary. Thus the CV birth rate for the mass-ratio distribution of uncorrelated component masses is higher than for a constant mass-ratio distribution. In addition, the CV birth rate decreases with increasing α_{CE} and α_{th}, since higher values of α_{CE} and α_{th} produce many more wide WD binaries after the CE phase whose orbits will not shrink significantly.

6.8 The formation of DDs and Type Ia SNe

Double degenerates form after one or two CE phases. The highest DD birth rate for our Galaxy in our simulations is 0.05 yr^{-1} (see Table 2). This rate is very sensitive to α_{CE}, α_{th}

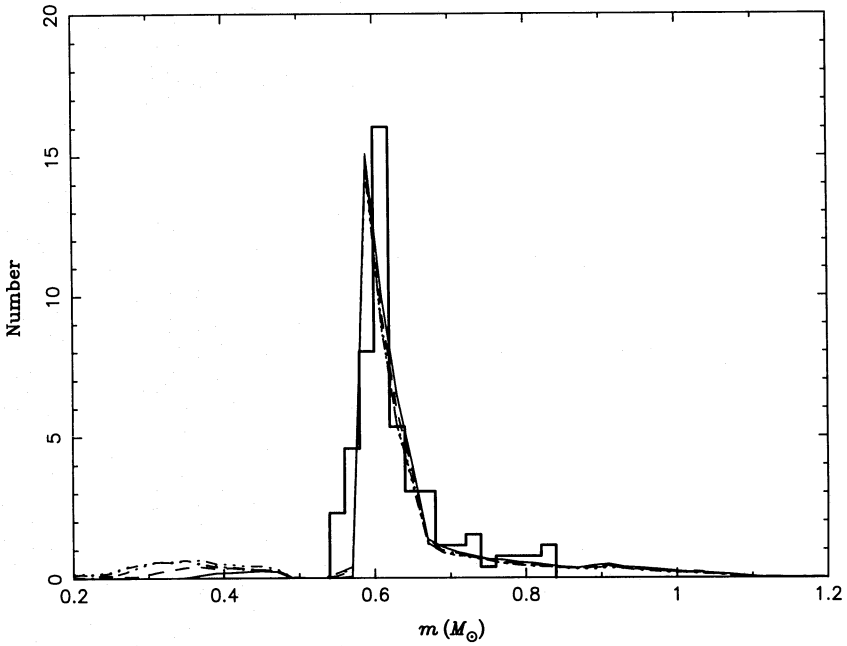

Figure 3. The distribution of masses of PN nuclei (white dwarfs) for simulations 1, 4, 6, 7, 13 (solid, dashed, dash–dotted, dotted, dash-dot-dot-dotted curves, respectively), compared with the observational distribution (Zhang & Kwok 1993; thick solid curve).

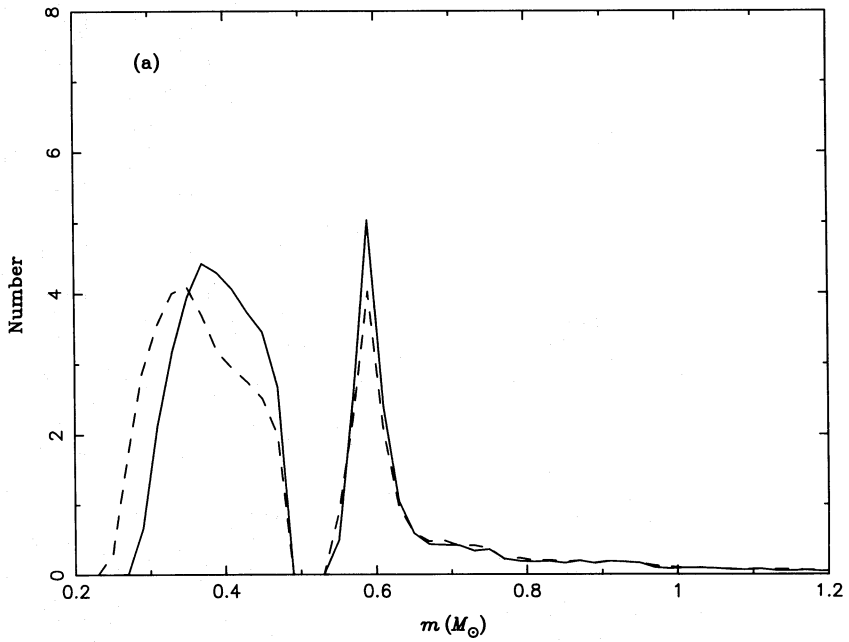

Figure 4. The distribution of WD masses (a), ratio of secondary to white dwarf mass (b) and orbital periods (c) for post CE systems. Solid curve: simulation 4; dashed curve: simulation 6.

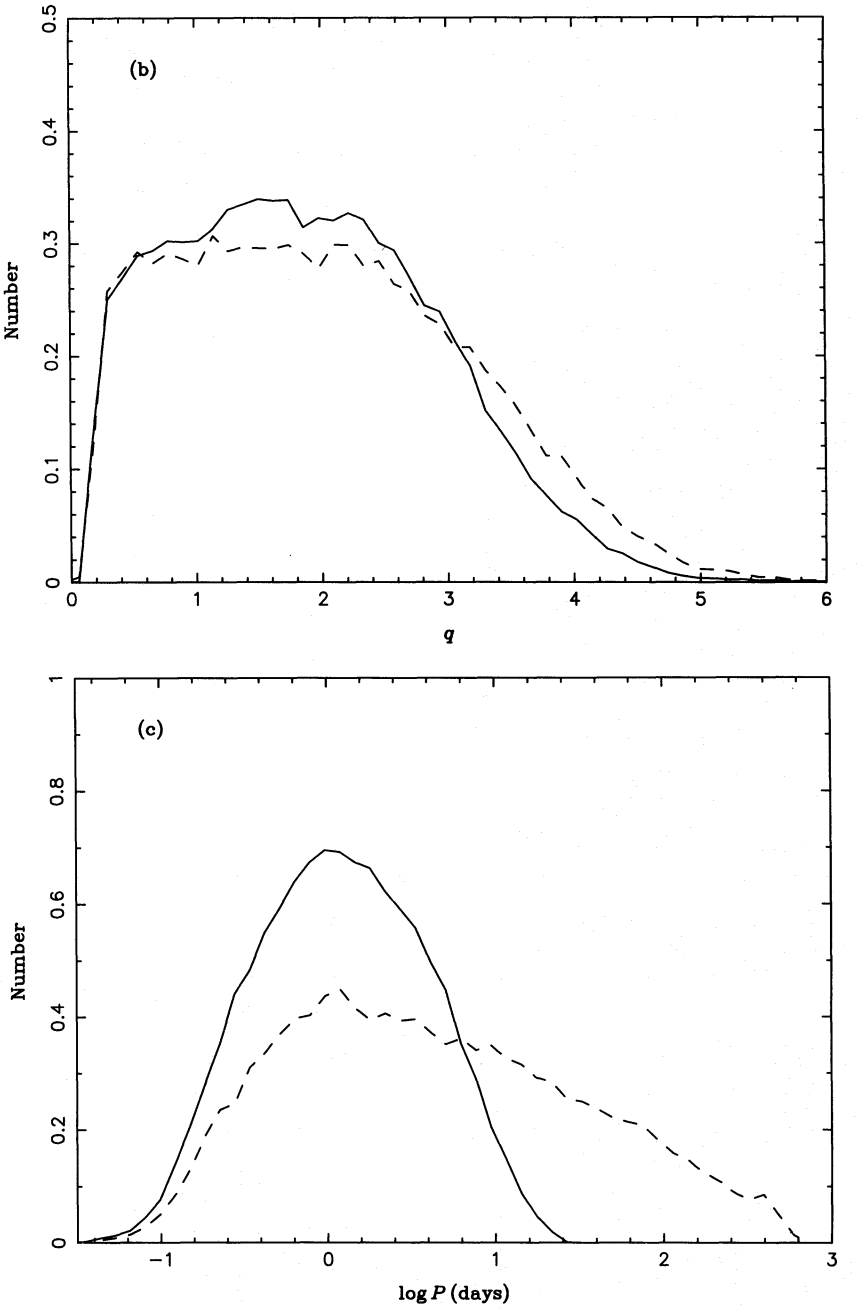

Figure 4 – *continued*

and the mass-ratio distribution. For larger α_{CE} and α_{th}, it is easier to eject the common envelope and to form a DD. For a constant or rising mass-ratio distribution, the secondary is, on average, more massive and more likely to experience a second CE phase, making the formation of a DD more likely.

Fig. 6 shows the distributions of primary masses, mass ratios, and orbital periods for simulations 4 and 6. Again we see that including the thermal energy in the calculation of envelope binding energy (simulation 6) tends to produce DDs with longer orbital periods.

If the two degenerate components merge due to the loss of angular momentum by gravitational radiation, this produces a single merged object or, perhaps in some cases, a Type Ia SN. The highest total DD merging rate in our simulations is 0.026 yr^{-1}; this rate is dominated by mergers of two helium white dwarfs, which may lead to the formation of O/B subdwarfs (Iben & Tutukov 1984a). The highest rate for the merger of a CO white dwarf with a helium white dwarf is 0.007 yr^{-1}. The highest merger rate of two CO white dwarfs with a total mass exceeding the Chandrasekhar mass and possibly producing a Type Ia supernova (Iben & Tutukov 1984b; Webbink & Iben 1987) is about 0.002 yr^{-1}.

6.9 Comparison with observations

Our simulations predict that up to ~ 17 per cent of PNe have close binary cores (with periods less than a few days); the

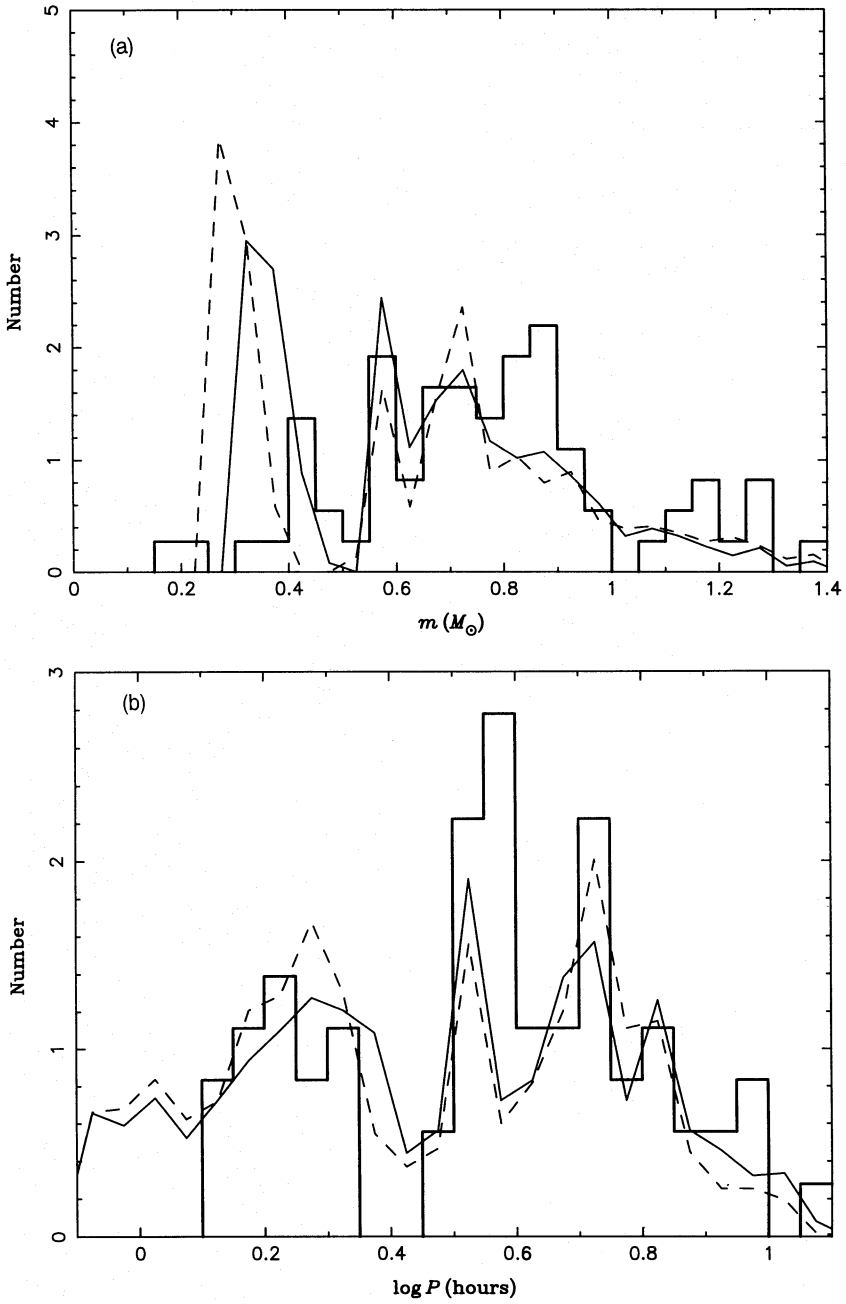

Figure 5. The distribution of masses of WDs (a) and initial periods (b) in CVs at the beginning of RLOF. Solid curve: simulation 4; dashed curve: simulation 6; thick solid curve: distribution of Ritter & Kolb (1994).

observed value is actually very close to this maximum value: ~17 per cent (Livio 1992), suggesting either that the observed sample is more or less complete or that the overall binary frequency should be higher (the alternative, that α_{CE} is larger than 1, is perhaps less attractive, since this would require an additional unknown energy source; see, for example, Livio 1994). We also predict that the structure of 34–43 per cent of PNe should be affected by binary interactions. This estimate is similar to the fraction of observed bipolar PNe (~50 per cent). We therefore conclude that binary interactions are likely to be one of the major factors in explaining the structure of very asymmetric PNe. The fraction of bipolar PNe could be substantially larger, if many stars have massive planets, since a massive planet spiralling into the envelope of an evolved star may be sufficient to spin-up the envelope and produce a non-spherical PN (Livio 1992, 1994). The distribution of masses of PN nuclei (Fig. 3) agrees well with the observational distributions (Zhang & Kwok 1993; their fig. 1). Zuckerman & Gatley (1988) have argued that strongly bipolar PNe tend to be found at lower galactic latitudes than the average PN, which suggests that bipolar PNe are connected with more massive stars. This is also consistent with our simulations, provided that the binary mass-ratio distribution is flat or rising towards 1.

The predicted CV birth rate, $(0.08\text{–}2)\times10^{-14}$ pc^{-3} yr^{-1}, is consistent with the inferred birth rate of $(1\text{–}2)\times10^{-14}$ pc^{-3} yr^{-1} (Ritter & Burkert 1986). Fig. 5(a) compares the distribution of WD masses in CVs as inferred from observations [from the CV catalogue of Ritter & Kolb (1994); note, however, that only a few of the masses in the catalogue are based directly on observations, i.e. come from systems that are eclipsing, double-lined spectroscopic binaries, and are therefore not without an element of hypothesis]. Considering the large observational uncertainties in WD masses and the presence of some strong observational selection effects (e.g. a CV with a lower WD mass has lower luminosity and is not so easily observed), we think that the distributions in our simulations (Fig. 5) are consistent with the observational one.

The birth rate of DD systems (Table 2) in our model Galaxy can be as high as 0.05 yr^{-1}; this is consistent with the upper limits (0.04–0.07) deduced from observations: for example 0.05 yr^{-1} (Robinson & Shafter 1987), 0.04–0.07 yr^{-1} (Bragaglia et al. 1991).

The merger of two CO white dwarfs with a total mass larger than the Chandrasekhar limit may lead to a Type Ia supernova (Iben & Tutukov 1984b; Webbink & Iben 1987). The highest Type Ia supernova frequency for our Galaxy that we predict according to this model is $\sim2\times10^{-3}$ yr^{-1}. This

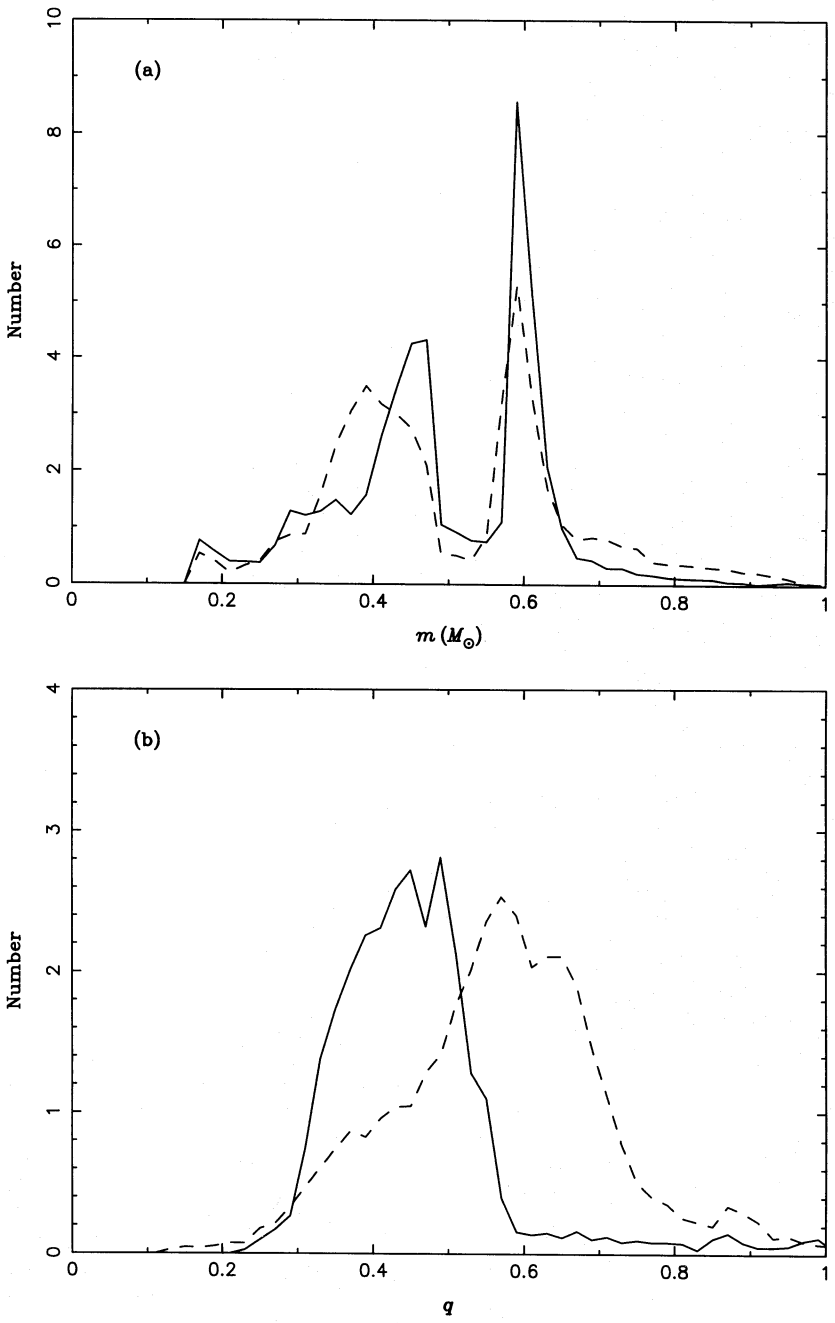

Figure 6. The distribution of primary masses (a), mass ratio (b) and orbital periods (c) for DD systems at birth. Solid curve: simulation 4; dashed curve: simulation 6.

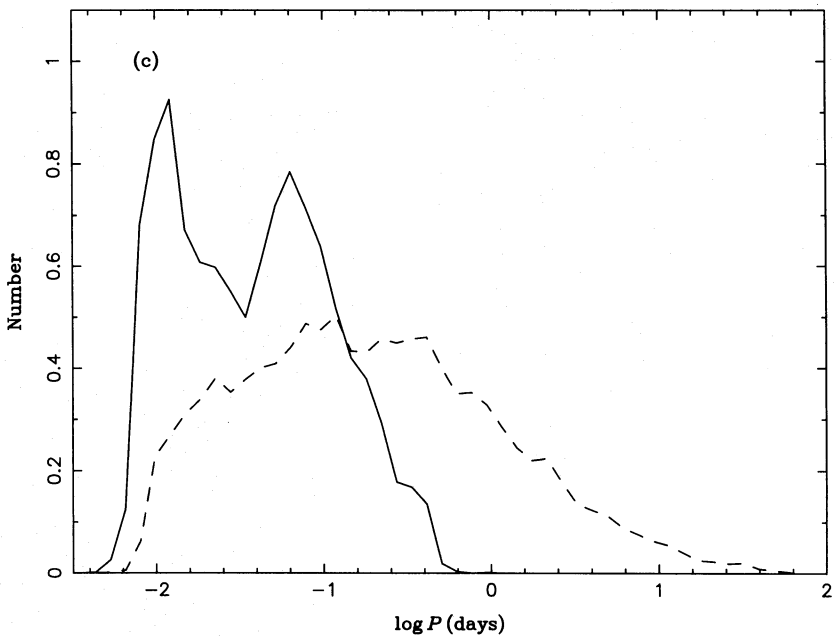

Figure 6 – *continued*

frequency is probably consistent with the observational frequency estimated as $(3\text{–}4)\times10^{-3}$ yr^{-1} by van den Bergh & Tammann (1991). However, for most of our simulations, the frequency is substantially smaller, typically $\lesssim10^{-3}$ yr^{-1}; this appears not to be consistent with the observed frequency. In these cases, one needs either a more efficient mechanism for orbital angular momentum loss during the CE or DD phase or a different evolutionary scenario for Type Ia supernovae altogether.

6.10 Comparison with the work of Yungelson et al. (1994)

In a series of papers, Iben, Tutukov and their collaborators have systematically explored the large variety of possible binary interactions. Among many other things, they have also investigated the formation of PNe and Type Ia supernovae via various binary channels (e.g. Iben & Tutukov 1984a,b, 1993; Tutukov et al. 1992; Yungelson et al. 1993, 1994). The results of the present study are in overall agreement with these studies. There are, however, also some significant differences, which we will discuss now. They illustrate the still substantial gaps in our understanding of certain aspects of binary evolution, in particular of common-envelope evolution.

(i) In their calculations, Iben and collaborators assume that a common envelope always forms when the mass donor is a post-main-sequence star, irrespective of whether mass transfer occurs on a thermal or a dynamical time-scale. This need not be the case when the mass donor is a star in the Hertzsprung gap, however, where it has a radiative envelope, provided that the mass ratio is not too large; see, for example, the detailed calculations of close binary evolution by van der Linden (1987). In our simulations we assume that, if the primary first fills its Roche lobe while it traverses the Hertzsprung gap, RLOF will not result in a common envelope, but in the transfer of the whole envelope of the primary to the secondary, leaving a naked helium core as remnant. The mass of the helium core is taken as the core mass of a star of the same initial mass at the beginning of the red giant branch.

On the other hand, if the accreting star is a degenerate star, the formation of a common envelope becomes very likely. We assume that a common envelope forms when the thermal time-scale mass-transfer rate, estimated according to the formalism of Rappaport, Verbunt & Joss (1983), exceeds the Eddington accretion rate of the degenerate star. This is only an approximate criterion since the accreting object will start to swell up at an accretion rate which may be substantially less than the Eddington rate (e.g. Nomoto 1982). This does not, however, automatically lead to a common-envelope phase, since the binary may be very efficient in ejecting matter from the system, which can, in principle, prevent the formation of a common envelope altogether. In our simulations, we find that, in the case of a degenerate accretor, the mass-transfer rate is generally so large that a common-envelope phase becomes unavoidable. Thus, in practice, our formalism only differs from the Iben et al. treatment in the case of non-degenerate accretors. This has, however, significant consequences for the total number of bipolar PNe (see the discussion in 6.2), the frequency of DDs and the frequency of the various merger events (6.8).

(ii) One of the most significant differences is in the definition of $\alpha_{\rm CE}$. Yungelson et al. (1994) define it by the equation

$$\frac{(M_1+M_2)(M_1-M_{1\rm R})}{A_0}=\alpha_{\rm CE}M_{1\rm R}M_2\left(\frac{1}{A_{\rm f}}-\frac{1}{A_0}\right), \qquad (13)$$

where M_1 and M_2 are the masses of the primary and secondary, respectively, $M_{1\rm R}$ is the remnant mass of the donor (primary) following the CE phase, and A_0 and $A_{\rm f}$ are the initial and final separations, respectively. The left side of equation (13) gives an estimate of the binding energy of the

common envelope, and the radius of the common envelope is taken as A_0; this is, however, much larger than the radius of the giant when it fills its Roche lobe (typically by a factor of 3) and therefore reduces the binding energy by a factor of about 3 in a somewhat artificial way (note that, even though the size of the initial common envelope may be about A_0, it will contain only very little mass at this stage). In other words, α_{CE} defined in this way gives a much higher actual CE ejection efficiency than the value of α_{CE} defined by our equation (8), or the similar definitions used by Webbink (1984) and de Kool (1990, 1992). In our work, the common-envelope binding energy is taken to be the envelope energy when the mass donor fills its Roche lobe and starts to transfer mass on a dynamical time-scale. The case of $\alpha_{CE} = 1$ in Yungelson et al. (1994) is then roughly equivalent to the case of $\alpha_{CE} \sim 3$ in our calculations.

Our results for the formation of bipolar PNe are similar to those of Yungelson et al. (1993). However, we obtain fewer binary systems consisting of a CO white dwarf and a main-sequence companion, and more consisting of a He white dwarf and a main-sequence companion after the CE phase. This is mainly due to the different treatments of the CE phase and the different adopted core mass–radius relations.

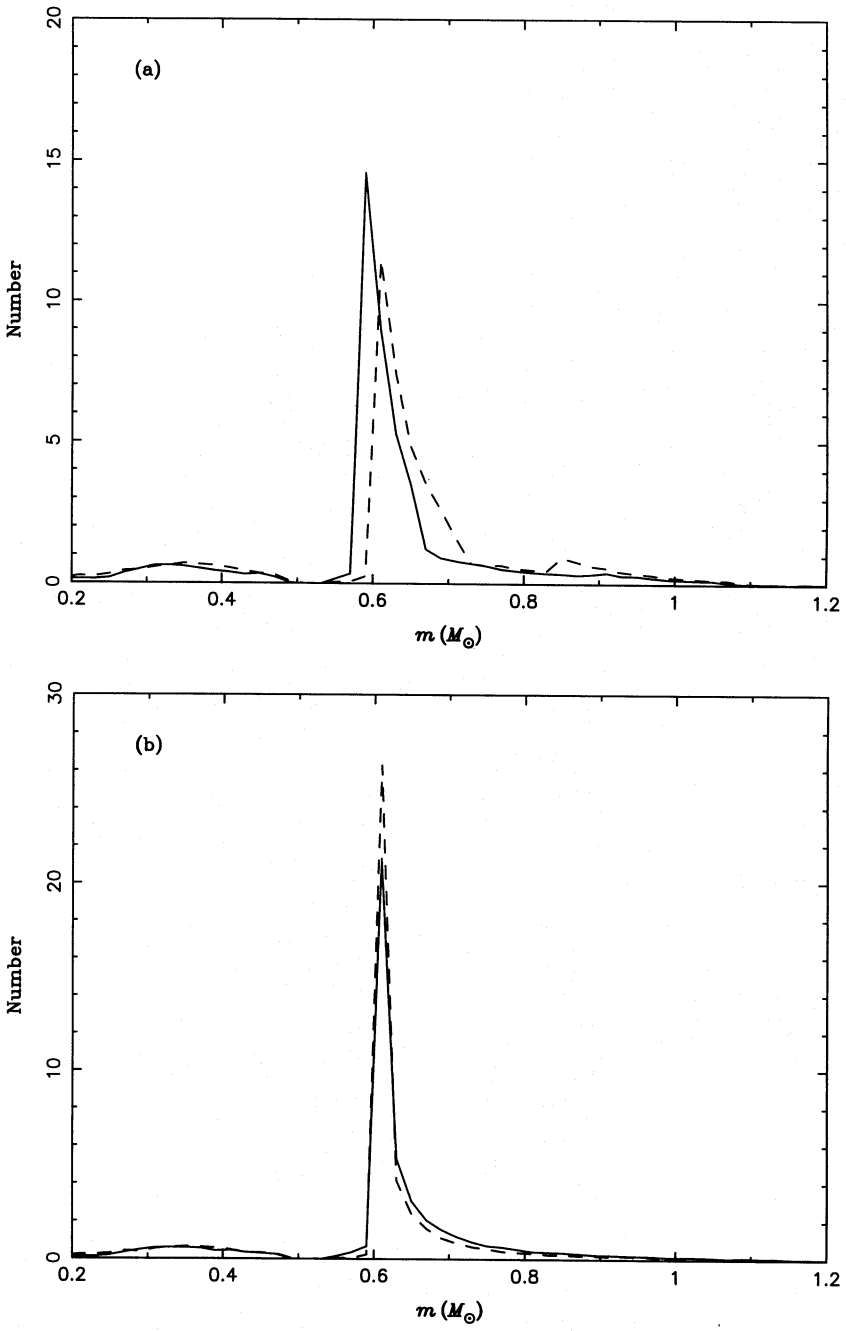

Figure 7. The distribution of masses of PN nuclei for Pop I (solid curve) and Pop II (dashed curve). a: HPE relation; b: YTL relation; c: IT relation.

Yungelson et al. (1993) use the core (He core, CO core and ONe core) mass–radius relations of Iben & Tutukov (1984a), whereas we obtain the relation by interpolation in our model grid. In our case, the radius corresponding to the same core mass is smaller for intermediate-mass stars and larger for low-mass stars. For example, our stellar radius is larger by a factor of 1.3 for a 0.48-$M_\odot$ He core of a 1-$M_\odot$ star and by a factor of 1.5 for a 0.60-$M_\odot$ CO core of a 1-$M_\odot$ star. As a consequence, overall we obtain more cases of CE evolution on the FGB and fewer on the AGB (since the IMF favours low-mass stars). For the same reason, our simulations produce more He white dwarf binaries and fewer CO white dwarf binaries.

Our Type Ia SN rate is smaller than that obtained by Yungelson et al. (1994). This is probably due to the fact that they adopted $\alpha_{CE} = 1$, which, as discussed above, is roughly a factor of 3 larger than the largest value we used.

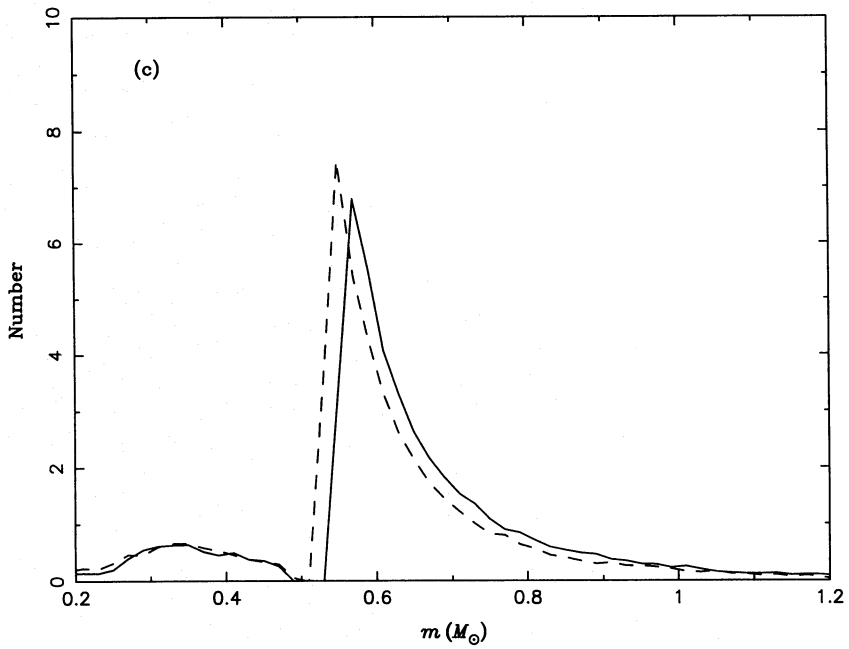

Figure 7 – *continued*

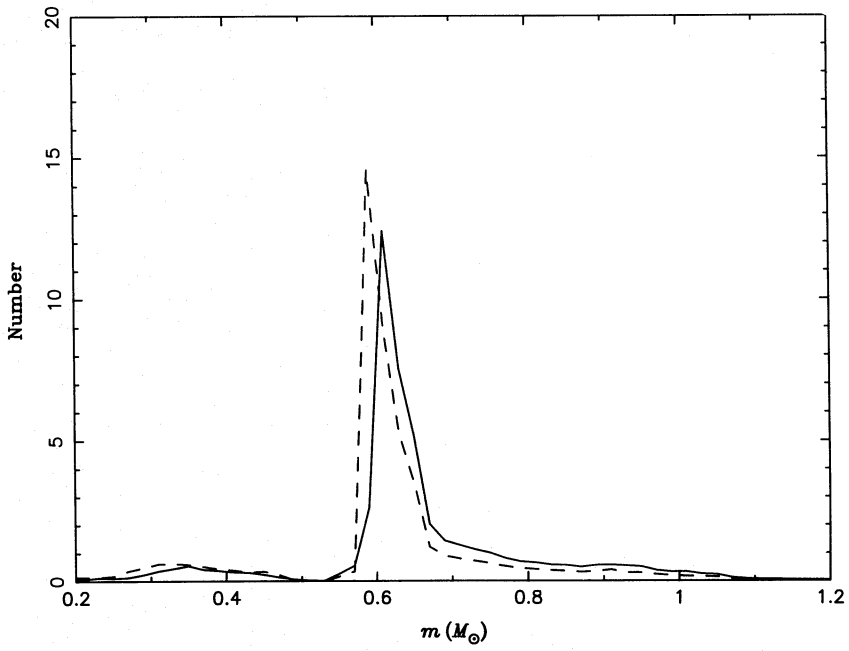

Figure 8. The distribution of masses of PN nuclei for different population ages (Pop I with HPE relation). Solid curve: 5 Gyr; dashed curve: 15 Gyr.

6.11 'Best model'

Simulations 6 and 7 appear to be in best agreement with the various observational constraints. They reproduce well the birth rate of CVs, the fraction of PNe with close binary cores, the fraction of bipolar PNe, and the DD birth rate. The SN Ia frequency (in the white dwarf merger model) is also marginally consistent, albeit perhaps slightly too low. Thus our preferred model has $\alpha_{CE}=1$, $\alpha_{th}=1$ and a constant or rising mass-ratio distribution. While we can not firmly rule out other values, considering the number of uncertain factors in the simulations, this suggests that the CE ejection process is very efficient, consistent with the conclusions of de Kool (1990) and Yungelson et al. (1994). We now use these preferred values to investigate the influences of metallicity, population age and initial–final mass relations with the constant mass-ratio distribution.

6.12 The influence of metallicity

As Table 3 shows, the fraction of bipolar PNe for Pop II is slightly lower than for Pop I. The fraction of PNe with close

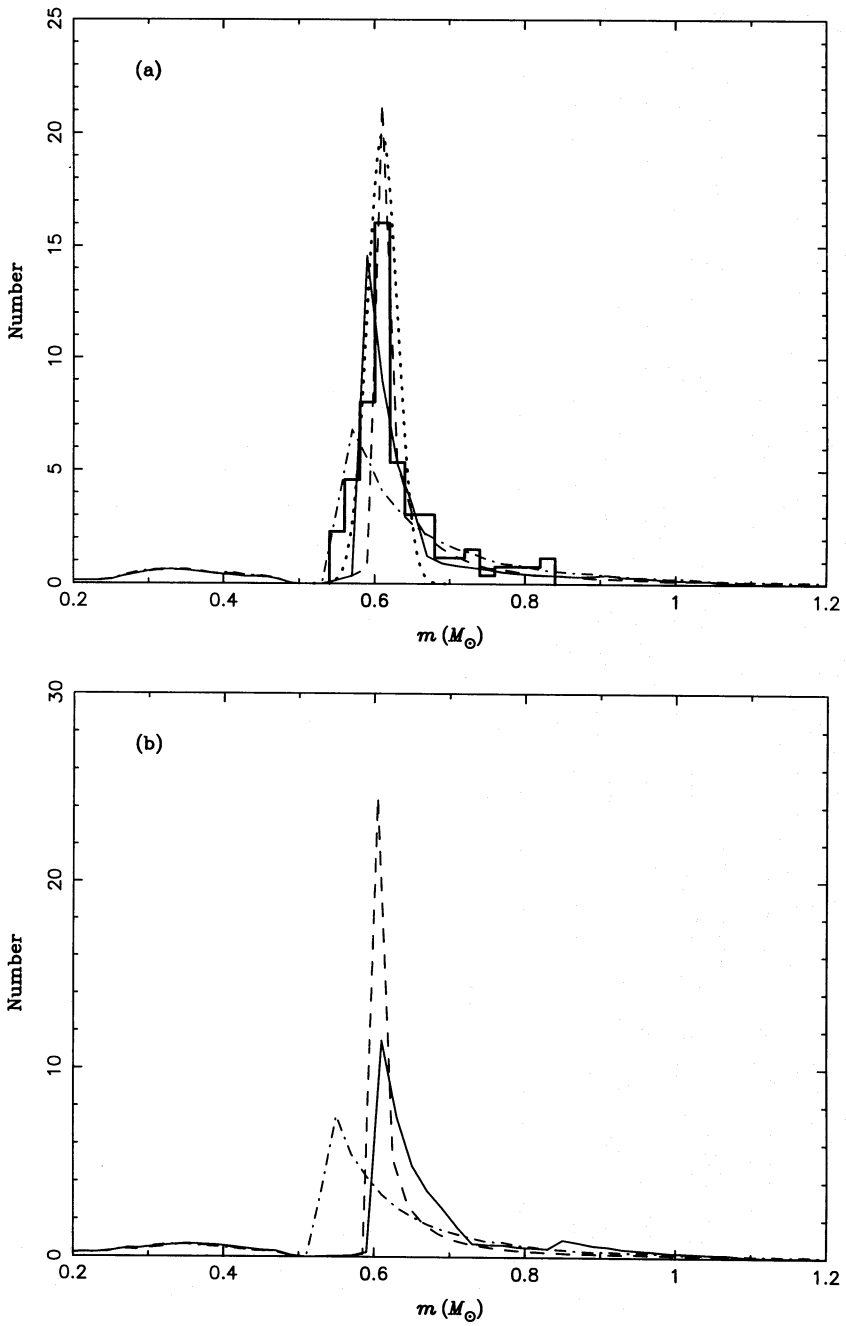

Figure 9. The distribution of masses of PN nuclei for different initial–final mass relations. Solid curve: HPE; dashed curve: YTL; dash–dotted curve: IT. (a): Pop I [thick solid curve: observations of Zhang & Kwok (1993); thick dotted curve: distribution inferred from observations by Jacoby (1989)], (b): Pop II.

binary nuclei for Pop II is slightly higher than for Pop I for the HPE relation, and is slightly smaller for the YTL and IT relations. The reason for these differences is that the HPE relation terminates the AGB evolution later for Pop II stars, whereas we used the same YTL or IT relation for Pop II as for Pop I. Similarly, the CV birth rates and DD birth rates are higher for Pop II with the HPE relation (Table 4).

The distribution of masses of PN nuclei peaks at a higher mass for Pop II with the HPE relation (0.61 ± 0.03 $M_\odot$ for Pop II, 0.59 ± 0.02 $M_\odot$ for Pop I), is almost unchanged with the YTL relation (0.60 ± 0.02 $M_\odot$), and is at a lower mass with the IT relation (0.54 ± 0.05 $M_\odot$ for Pop II and 0.56 ± 0.05 $M_\odot$ for Pop I), as seen in Figs 7(a)–(c).

6.13 The influence of age

Massive binaries are more important for younger populations. Therefore the fraction of bipolar PNe increases with decreasing age, while the fraction of PNe with close binary nuclei and the CV and DD birth rates decrease.

The distribution of masses of PN nuclei peaks at a higher mass for a younger population: 0.60 ± 0.03 $M_\odot$ for Pop I with an age of 5 Gyr and the HPE relation, 0.59 ± 0.02 $M_\odot$ with an age of 15 Gyr, as shown in Fig. 8.

6.14 The influence of the initial–final mass relation

For Pop I, the results are very similar for the three differential initial–final mass relations. Since the IT relation terminates the AGB evolution slightly later for massive stars, it leads to a slightly higher fraction of bipolar PNe, slightly more PNe with close binary nuclei, and slightly higher CV and DD birth rates.

For Pop II, however, the differences between the different relations are quite significant, mainly because the HPE relation terminates the AGB evolution much later (i.e. at higher core masses) than the YTL or IT relations, and thus leads to a higher bipolar PN fraction, more PNe with close binary nuclei (due to an increase of AGB CE ejection cases), and an increase of the DD birth rate.

The distributions of masses of PN nuclei for the different initial–final mass relations are shown in Fig. 9. For Pop I, the distribution with the YTL relation is sharper and peaks at 0.60 ± 0.02 $M_\odot$, the distributions with the HPE and IT relations peak at 0.59 ± 0.02 $M_\odot$ and 0.56 ± 0.05 $M_\odot$, respectively. For Pop II, the distributions peak at 0.60 ± 0.02 $M_\odot$, 0.61 ± 0.03 $M_\odot$, and 0.54 ± 0.05 $M_\odot$ for the YTL, HPE and IT relations, respectively.

The distribution with the HPE relation gives better agreement with the observations of Zhang & Kwok, as well as with the distribution inferred observationally by Jacoby (1986) – see Fig. 9. While these observationally inferred masses must still be considered somewhat uncertain, they provide some observational support for the HPE relation.

6.15 PNe as distance indicators

The PN luminosity function may provide an important standard candle for distance determinations as proposed by Jacoby (1986) and his collaborators. The main requirements of this method are (1) that the distribution of masses of the central nuclei of PNe has a sharp and well-defined peak and (2) that the location of the peak is not a very sensitive function of the parameters, such as age and metallicity, of the underlying stellar population. Our simulations (Figs 3, 7, 8 and 9) suggest that both of these requirements are fulfilled, although the location of the peak should depend on the metallicity of the population through the metallicity dependence of the initial–final mass relation (as predicted by HPE).

7 CONCLUSIONS

The main conclusion of this study is that we expect that binary interactions affect the shaping of some 40 per cent of all PNe. Since this fraction is comparable to the fraction of very non-spherical PNe, binary interactions are likely to be a major, if not the single most important, factor in explaining the very asymmetric PNe. We also found that the three main binary channels, binary gravitational focusing, common-envelope ejection and binary merger, are all of comparable importance. The resulting stellar systems are, however, quite different, consisting of wide binaries in the first case (with orbital periods of years to decades), very close binaries in the second case (with orbital periods of days to hundreds of days) and single white dwarfs in the third case. Our simulations also predict birth rates for binary PN nuclei, CVs and DDs which appear to be in overall agreement with the observationally deduced rates, providing an independent check of our model assumptions. There are still substantial uncertainties in the properties and statistics of binary systems and large gaps in our theoretical understanding of certain critical phases of binary evolution. We suspect, however, that our basic conclusions are not strongly affected by these uncertainties.

ACKNOWLEDGMENT

ZH is grateful to the British Council for the award of a Research Studentship.

REFERENCES

Abt H. A., Levy S. G., 1976, ApJS, 30, 273
Abt H. A., Levy S. G., 1978, ApJS, 36, 241
Bond H. E., Livio M., 1990, ApJ, 355, 568
Bopp B. W., Stencel R. E., 1981, ApJ, 247, L131
Bragaglia A., Greggio L., Renzini A., D'Odorico S., 1991, in Woosley S. E., ed., Supernovae. Springer, New York, p. 599
Bragaglia A., Renzini A., Bergeron P., 1993, in Barstow M. A., ed., White Dwarfs: Advances in Observation and Theory. Kluwer, Dordrecht, p. 325
Chevalier R. A., Luo D., 1994, ApJ, 421, 225
de Kool M., 1990, ApJ, 358, 189
de Kool M., 1992, A&A, 261, 188
Duquennoy A., Mayor M., 1990, A&A, 248, 485
Eggleton P. P., 1976, in Eggleton P. P., Mitton S., Whelan J., eds, Proc. IAU Symp. 73, Structure and Evolution of Close Binary Systems. Reidel, Dordrecht, p. 209
Eggleton P. P., Tout C. A., 1989, in Batten A. H., ed., Proc. IAU Colloq. 107, Algols. Kluwer, Dordrecht, p. 164
Eggleton P. P., Fitchett M. J., Tout C. A., 1989, ApJ, 347, 998
Fabian A. C., Hansen C. J., 1979, MNRAS, 187, 283
Frank A., Balick B., Icke V., Mellema G., 1993, ApJ, 404, L25
Garcia J. M., Gimenez A., 1992, in Kondo Y., Sistero R. F., Polidan R. S., eds, Proc. IAU Symp. 151, Evolutionary Processes in Interacting Binary Stars. Kluwer, Dordrecht, p. 337
Goldberg D., Mazeh T., 1994, A&A, 282, 801

Han Z., Podsiadlowski Ph., Eggleton P. P., 1994a, in D'Antona F., Caloi V., Maceroni C., Giovanelli F., eds, Evolutionary Links in the Zoo of Interacting Binaries. Mem. Soc. Astron. Ital., 65, 407
Han Z., Podsiadlowski Ph., Eggleton P. P., 1994b, MNRAS, 270, 121 (HPE)
Hjellming M. S., Webbink R. F., 1987, ApJ, 318, 794
Iben I., Jr, Tutukov A. V., 1984a, ApJS, 54, 335 (IT)
Iben I., Jr, Tutukov A. V., 1984b, in Chiosi C., Renzini A., eds, Stellar Nucleosynthesis. Reidel, Dordrecht, p. 181
Iben I., Jr, Tutukov A. V., 1993, ApJ, 418, 343
Icke V., Preston H. L., Balick B., 1989, AJ, 97, 462
Jacoby G. H., 1989, ApJ, 339, 39
Kahane C., Maizels C., Jura M., 1988, ApJ, 328, L25
Kahn F. D., West K. A., 1985, MNRAS, 212, 837
Kolb U., 1993, A&A, 271, 149
Kolesnik I. G., Pilyugin L. S., 1986, SvA, 30, 169
Kraicheva Z. T., Popova E. I., Tutukov A. V., Yungelson L. R., 1978, SvA, 22, 670
Kraicheva Z. T., Popova E. I., Tutukov A. V., Yungelson L. R., 1979, SvA, 23, 290
Kwok S., 1982, ApJ, 258, 280
Kwok S., Purton C. R., Fitzgerald P. M., 1978, ApJ, 219, L125
Landau L. D., Lifshitz E. M., 1962, The Classical Theory of Fields. Pergamon, Oxford
Livio M., 1992, in Weinberger R., Acker A., eds, Proc. IAU Symp. 155, Planetary Nebulae. Kluwer, Dordrecht, p. 279
Livio M., 1994, in Clegg R. S., Stevens I. R., Meikle W. P. S., eds, Circumstellar Media in the Late Stages of Stellar Evolution. Cambridge Univ. Press, Cambridge, p. 35
Livio M., Soker N., 1988, ApJ, 329, 764
Livio M., Salzman J., Shaviv G., 1979, MNRAS, 188, 1
Mazeh T., Goldberg D., Duquennoy A., Mayor M., 1992, ApJ, 401, 265
Miller G. E., Scalo J. M., 1979, ApJS, 41, 513
Morbey C. J., Griffin R. F., 1987, ApJ, 317, 343
Morris M., 1981, ApJ, 249, 572
Morris M., 1987, PASP, 99, 1115
Morris M., 1990, in Mennessier M. O., Omont A., eds, From Miras to Planetary Nebulae: Which Path for Stellar Evolution? Editions Frontières, Gif-sur-Yvette, p. 520
Morton D. C., 1960, ApJ, 132, 146
Nomoto K., 1982, ApJ, 253, 798
Nomoto K., Iben I., Jr, 1985, ApJ, 297, 531
Okorokov V. A., Shustov B. M., Tutukov A. V., Yorke H. W., 1985, A&A, 142, 441
Paczyński B., 1971, Acta Astron., 21, 1
Paczyński B., 1985, in Lamb D. Q., Patterson J., eds, Cataclysmic Variables and Low-Mass X-Ray Binaries. Reidel, Dordrecht, p. 1
Paczyński B., Sienkiewicz R., 1972, Acta Astron., 22, 73
Pascoli G., 1987a, A&A, 180, 191
Pascoli G., 1987b, Ap&SS, 134, 73
Pikel'ner S. B., 1968, ApJ, 2, L97
Pikel'ner S. B., 1973, ApJ, 15, L91
Pilyugin L. S., 1987, SvA, 31, 282
Podsiadlowski Ph., Clegg R. E. S., 1992, in Gondhalekar P. M., ed., Proc. Workshop on Astronomy and Astrophysics "Dusty Disks". RAL, Didcot, p. 69
Podsiadlowski Ph., Joss P. C., Hsu J. J. L., 1992, ApJ, 391, 246
Poe C. H., Friend D. B., 1986, ApJ, 311, 317
Rappaport S., Verbunt F., Joss P. C., 1983, ApJ, 275, 713
Reimers D., 1975, Mem. Soc. Roy. Sci. Liège 6e Ser., 8, 369
Ritter H., Burkert A., 1986, A&A, 158, 161
Ritter H., Kolb U., 1994, in Lewin W. H. G., van Paradijs J., van den Heuvel E. P. J., eds, X-ray Binaries. Cambridge Univ. Press, Cambridge, in press
Robinson E. L., Shafter A. W., 1987, ApJ, 322, 296
Rogers F. J., Iglesias C. A., 1992, ApJS, 79, 507
Saffer R. A., Liebert J., Olszewski E., 1988, ApJ, 334, 947
Soker N., Livio M., 1989, ApJ, 339, 268
Sparks W. M., Stecher T. P., 1974, ApJ, 188, 149
Tout C. A., Eggleton P. P., 1988, ApJ, 334, 357
Tutukov A. V., Yungelson L. R., Iben I., Jr, 1992, ApJ, 386, 197
van den Bergh S., Tammann G. A., 1991, ARA&A, 29, 363
van der Linden T. J., 1987, A&A, 178, 170
Verbunt F., Zwaan C., 1981, A&A, 100, L7
Volk K. M., Kwok S., 1985, A&A, 153, 79
Webbink R. F., 1984, ApJ, 277, 355
Webbink R. F., 1986, in Leung K.-C., Zhai D.-S., eds, Critical Observations versus Physical Models for Close Binary Systems. Gordon & Breach, New York, p. 403
Webbink R. F., 1988, in Mikołajewska J., Friedjung M., Kenyon S. J., Viotti R., eds, The Symbiotic Phenomenon. Kluwer, Dordrecht, p. 311
Webbink R. F., Iben I., Jr, 1987, in Philip A. G. D., Hayes D. S., Liebert J. W., eds, Proc. IAU Colloq. 95, The Second Conference on Faint Blue Stars. L. Davis Press, Schenectady, p. 445
Weidemann V., 1984, A&A, 134, L1
Weidemann V., 1990, ARA&A, 28, 103
Weidemann V., Koester D., 1983, A&A, 121, 77
Weiss A., Keady J. J., Magee N. H., Jr, 1990, Atomic Data and Nuclear Data Tables, 45, 209 (WKM)
Yungelson L. R., Tutukov A. V., Livio M., 1993, ApJ, 418, 794 (YTL)
Yungelson L. R., Livio M., Tutukov A. V., Saffer R. A., 1994, ApJ, 420, 336
Zhang C. Y., Kwok S., 1993, ApJS, 88, 137
Zuckerman B., Aller J. H., 1986, ApJ, 301, 772
Zuckerman B., Gatley I., 1988, ApJ, 324, 501